Journal of Drug Design and Medicinal Chemistry
2017; 3(6): 86-113
http://www.sciencepublishinggroup.com/j/jddmc
doi: 10.11648/j.jddmc.20170306.13
ISSN: 2472-355X (Print); ISSN: 2472-3576 (Online)

Research Article

In silico Design of Phosphonic Arginine and Hydroxamic Acid Inhibitors of *Plasmodium falciparum* M17 Leucyl Aminopeptidase with Favorable Pharmacokinetic Profile

Hermann N'Guessan[1], Eugene Megnassan[1, 2, *]

[1]Faculty of Fundamental and Applied Sciences (UFR SFA), Laboratoire de Physique Fondamentale et Appliquée, University Abobo Adjamé (Now Nangui Abrogoua), Abidjan, Cote D'Ivoire

[2]International Centre for Science and High Technology (ICS-UNIDO), Area Science Park, Trieste, Italy

Email address:
nerhminos@yahoo.fr (H. N'Guessan), megnase@yahoo.com (E. Megnassan)

[*]Corresponding author

To cite this article:
Hermann N'Guessan, Eugene Megnassan. *In silico* Design of Phosphonic Arginine and Hydroxamic Acid Inhibitors of *Plasmodium falciparum* M17 Leucyl Aminopeptidase with Favorable Pharmacokinetic Profile. *Journal of Drug Design and Medicinal Chemistry*. Vol. 3, No. 6, 2017, pp. 86-113. doi: 10.11648/j.jddmc.20170306.13

Received: November 17, 2017; **Accepted**: December 8, 2017; **Published**: January 11, 2018

Abstract: We virtually design here new subnanomolar range antimalarials, inhibitors of *plasmodium falciparum* M17 Aminopeptidase (*pf*A-M17), by means of structure-based molecular design. Complexation QSAR models were elaborated for two training sets (6 methylphosphonic acids (APP) resp. 13 Hydroxamic Acid derivatives (AHO): $QSAR_{APP}$. resp. $QSAR_{AHO}$) and a linear correlation was established between the computed Gibbs free energies of binding (GFE: $\Delta\Delta G_{com}$) and observed enzyme inhibition constants (K_i^{exp}) for each training set: $QSAR_{APP}$: $pK_i^{exp}=-0.1665\times\Delta\Delta G_{com}+7.9581$, $R^2=0.97$ resp. $QSAR_{AHO}$: $pK_i^{exp}=-0.4626\times\Delta\Delta G_{com}+8.1842$, $R^2=0.98$. The predictive power of the QSAR models was validated with 3D-QSAR pharmacophore generation (PH4): $PH4_{APP}$: $pK_i^{exp}=0.99677\times pK_i^{pred}-0.00457$, $R^2=0.99$ resp. $PH4_{AHO}$: $pK_i^{exp}=1.02016\times pK_i^{pred}-0.10478$, $R^2=0.99$. Breakdown of computed *pf*A-M17:APPs resp. *pf*A-M17:AHOs interaction energy into each active site residue's contribution provided additional helpful structural information to design new APP and AHO analogues in a consistent way. In a first step we designed a virtual library (VL_{APP} resp. VL_{AHO}) from P_1 and P'_1 substitutions to explore both S_1 and S'_1 pockets. Further the VLs screened with the 3D-QSAR PH4s and the K_i^{pred} of the best fit hits virtually evaluated with $QSAR_{APP}$ resp. $QSAR_{AHO}$ models. This approach combining use of molecular modeling, PH4 and *in silico* VL screening helpfully provided valuable structural information for the synthesis of novel pfA-M17 inhibitors.

Keywords: Drug Design, QSAR Model, Pharmacophore Model, ADME Properties, Complexation Model, Molecular Modelling

1. Introduction

Malaria, along with tuberculosis and HIV/AIDS are the major infectious diseases infecting hundred millions people each year at such a level that the United Nations raised their eradication as a Millennium Development Goal (MDG 6: "Combat HIV/AIDS, malaria and other diseases"). Recently UN MDG Report 2015 states: "The global malaria incidence rate has fallen by an estimated 37% and the mortality rate by 58%" [1]. This achievement is mainly attributed to the following facts: "More than 900 million insecticide-treated mosquito nets were delivered to malaria-endemic countries in sub-Saharan Africa between 2004 and 2014 …, //indoor residual spraying, //diagnostic testing and artemisinin-based combination therapies (ACT)" [1].

For one decade (2006 – 2016), survival of millions people at risk of malaria infection relies on the strategy of "ACT", the strength of which remains unable to address the unstoppably growing spread of artemisinin-resistant *Plasmodium falciparum* (*pf*) [2, 3] for long.

One alternative to ACT anti *pf* resistance strategy is the design of hybrid drugs where two antimalarial moieties are linked into a unique molecule, these moieties known for their confirmed antimalarial potency against two different parasite targets and operating according different mechanisms of action [4, 5, 6].

Another promising gate was opened through the identification and characterization of new parasite therapeutic targets such as metalloaminopeptidases (MAP), reported to play a crucial role in the parasite viability and survival [7, 8, 9]. Among them both M1 alanyl and M17 leucyl specific aminopeptidases (*pf*A-M1, *pf*A-M17) are validated ones, due to their mediation during the final stage of hemoglobin digestion were they split small peptide fragments into free amino acids and thereafter by their inhibition which is lethal to *pf* [10, 11] they are worth targeting.

The X-rays crystal structure analysis of *pf*A-M17 (PDB code 4K3N) active site reveals, besides the two catalytic zinc ions in coordination with Asp 459, Lys 374, Asp 379, Asp 399, Glu 461, also a narrow hydrophobic S1 pocket with residues Met 392, Met 396, Phe 398 (suitable for stacking interaction), Thr 486, Gly 489, Leu 492, and Phe 583 and no suitable polar hydrogen-bonding partners (acceptor or donor) to interact with any charged P1 sidechain [9, 12, 13] and finally a S1' cavity with hydrophobic residues namely Ala 460 and Ile 547.

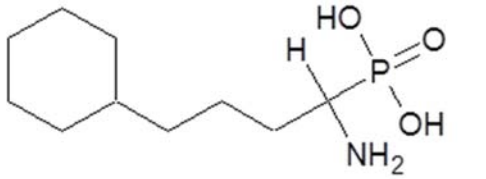

1 (14 μM)

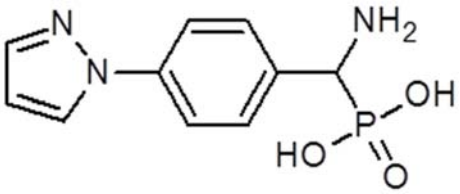

2 (11 nM)

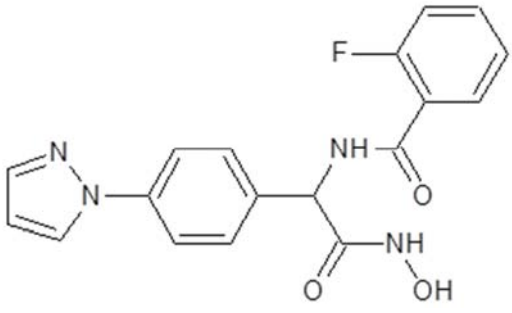

3 (8 nM)

Figure 1. *Chemical structure of antimalarial agents: Phosphinate dipeptide core (1), phosphonic arginine core (2) and amino-hydroxamic acid core (3).*

Phosphinate dipeptide analogue inhibitors of *pf*A-M17 reaching 14 μM (compound 1 in Figure 1) were identified first as lead antimalarials [7]. Thereafter phosphonic arginine inhibitors were designed ($K_i \geq 11$ nM) (compound 2 in Figure 1) probing the S1 pocket at the enzyme active site for a better insight into the interactions and structural requirements for nanomolar range potency [12]. X-rays crystal structure of *pf*A-M17 in complex with 2 confirmed these interactions particularly the coordination of 2 to the catalytic zinc ion through the aminophosphonate moiety [12]. More recently, the same authors extended their investigations by replacing the phosphonic acid Zinc Binding Group (ZBG) present in 2 with an aminohydroxamic acid analogue of aminophosphonic in order to probe the S1' pocket of *pf*A-M17 for additional affinity. This novel series allowed access to S1', improving the potency from 11 to 8 nM (compound 3, Figure 1) [13].

The structure activity relationship (SAR) from these studies and the availability of X-rays crystal structure *pf*A-M17 in complex with 2 and 3 respectively triggers an *in silico* attempt for the design of *pf*A-M17 inhibitors filling advantageously both S1 and S1' cavities.

In our present study, starting from high resolution 3D structure of *pf*A-M17 in complex with 2 and 3 respectively (PDB codes 4K3N and 4R76), we first elaborate two Molecular Mechanics Poisson-Boltzmann (MMPB) QSAR models of complexation of *pf*A-M17 first with aminophosphonic (APP) and then with aminohydroxamic (AHO) inhibitors respectively by computing the free energy of complexation (ΔG_{com}) for the Training Set (TS) which were correlated with the biological activity to explain about 98% of the variation of K_i values by that of ΔG_{com}. Besides a three dimensional quantitative structure-activity relationship (3D-QSAR) pharmacophore model was used to prepare a four-feature pharmacophore (PH4) of the bound APPs and AHOs respectively, which then was matched against the molecular data of the designed analogues to confirm the compliance with each QSAR model. Moreover, the computed enzyme – ligand interaction energy map E_{int} correlates well with K_i; thus allowing us to reach its breakdown to each active site residue contribution. From this last structural information we were able to select P1 and P1' suitable fragments as building blocks for a Virtual Library (VL) of *pf*A-M17 inhibitors. In order to prevent any toxicity issue and access good pharmacokinetic profile analogues, the VL was focused, prior to any screening, to those compounds the ADMET of which has 0 property descriptors that fall outside the range of values determined for 95% of known drugs out of 24 selected descriptors computed by the QikProp [14]. The predictability of the obtained QSAR models of inhibitor-enzyme binding cross-checked with a PH4 3D-QSAR pharmacophore model was used to screen the VL. The best Hit Fits from the PH4-based virtual screening of the VL have been *in silico* MMPB evaluated to yield a predicted inhibitory activity reaching the picomolar range for the most potent analogues.

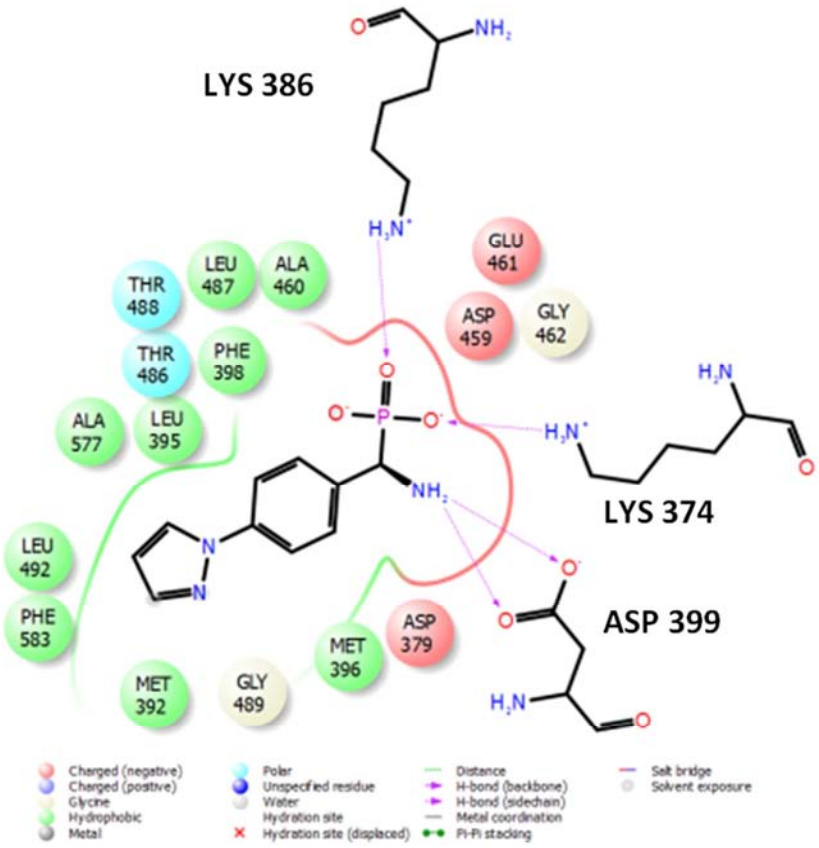
LYS 386
LYS 374
ASP 399
GLU 461
ASP 459
GLY 462
LEU 487
ALA 460
THR 488
THR 486
PHE 398
ALA 577
LEU 395
LEU 492
PHE 583
MET 396
ASP 379
MET 392
GLY 489
Charged (negative)
Charged (positive)
Glycine
Hydrophobic
Metal
Polar
Unspecified residue
Water
Hydration site
Hydration site (displaced)
Distance
H-bond (backbone)
H-bond (sidechain)
Metal coordination
Pi-Pi stacking
Salt bridge
Solvent exposure

(A)

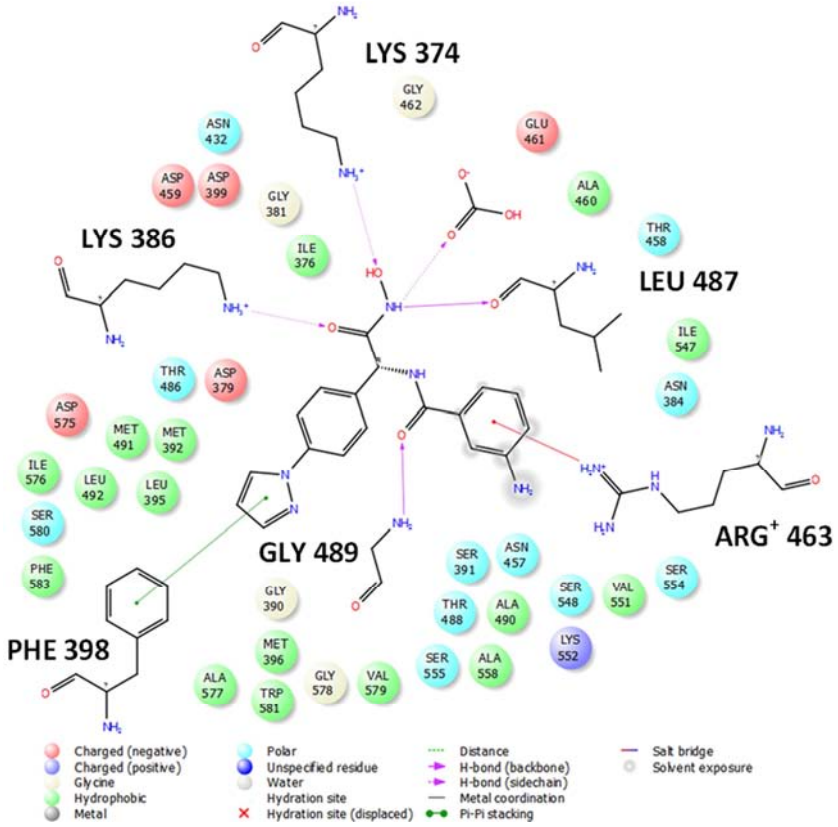
LYS 374
LYS 386
LEU 487
GLY 489
ARG+ 463
PHE 398
GLY 462
GLU 461
ASN 432
ASP 459
ASP 399
GLY 381
ALA 460
THR 458
ILE 376
ILE 547
ASN 384
THR 486
ASP 379
ASP 575
MET 491
MET 392
ILE 576
LEU 492
LEU 395
SER 580
PHE 583
SER 391
ASN 457
SER 554
GLY 390
SER 548
VAL 551
THR 488
ALA 490
LYS 552
MET 396
SER 555
ALA 558
ALA 577
GLY 578
VAL 579
TRP 581
Charged (negative)
Charged (positive)
Glycine
Hydrophobic
Metal
Polar
Unspecified residue
Water
Hydration site
Hydration site (displaced)
Distance
H-bond (backbone)
H-bond (sidechain)
Metal coordination
Pi-Pi stacking
Salt bridge
Solvent exposure

(B)

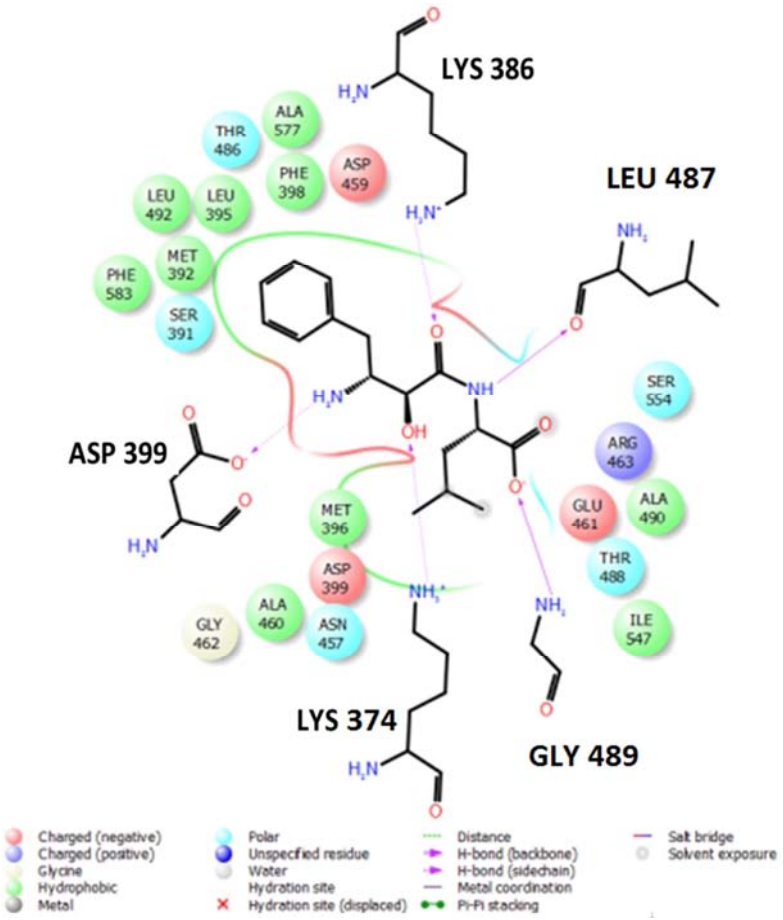

(C)

Figure 2. *pfA-M17– ligand interactions at active site depicted in 2D for the most active APP (A), AHO (B) and Bestatin (C) respectively.*

2. Methods

The complexation methodology has been described largely accor-ding to a procedure successfully used to elaborate one descriptor QSAR models of viral, bacterial and protozoal protease-inhibitor complexes and from them to design peptidomimetic, hydroxylnaphthoic, thymidine, triclosan and pyrrolidine carboxamide derivative inhibitors [15, 16, 17, 18, 19, 20, 21, 22, 23,24].

2.1. Training and Validation Sets

The training and validation sets of aminophosphonic and amino-hydroxamic analogues inhibitors of *pf*A-M17 used in this study were selected from literature [12, 13]. The inhibitory potencies of these derivatives cover sufficiently broad range of activity to allow reliable QSAR models to be built ($11 \leq K_i \leq 1000001$ nM and $8 \leq K_i \leq 501000$ nM respectively).

2.2. Model Building

Molecular models of free enzyme *pf*A-M17 (*E*), free inhibitors (*I*) and the enzyme-inhibitor complexes (*E*:*I*), were built from high-resolution crystal structure of the reference complex *pf*A-M17:APP1 and *pf*A-M17:AHO4 containing the APP1 and AHO4 respectively [12, 13] (Protein Data Bank [25] entry codes 4K3N and 4R76 at a resolution of 2 Å and 2.5 Å respectively) using the graphical user interface available in Insight-II molecular modeling program [26]. The most recent detailed description of this method is in ref. [23, 24].

2.3. Entropic Term

The most recent detailed description of the ligand vibrational entropic loss upon E:I complex formation and its use procedure in binding affinity calculation is available ref. [23].

2.4. Calculation of Binding Affinity

The calculation of binding affinity upon E:I complex formation according to the Molecular Mechanics and Poisson-Boltzmann scheme (MM-PB) is reported fully in refs. [23, 24].

2.5. Pharmacophore Generation

Pharmacophore modeling procedure as reported in [24] has been used in this work.

2.6. Interaction Energy

To calculate the MM interaction energy (E_{int}) between

enzyme residues and the inhibitor, a protocol available in Discovery Studio 2.5 [27] that computes the non-bonded interactions (van der Waals and electrostatic terms) between defined sets of atoms, was used. The calculations were performed using CFF force field [27] with a dielectric constant of 4. The breakdown of E_{int} into active site residue contributions (presented in% of total E_{int} of *pf*A-M17 – APP and *pf*A-M17 – AHO respectively) reveals the significance of individual interactions and allows a comparative analysis, which leads to identification of affinity enhancing and unfavorable APP and AHO substitutions.

2.7. ADME-Related Properties

The ADME-related properties treatment in this work has been fully described in [24].

2.8. Virtual Library Generation

The analogue model building was performed with Molecular Operating Environment (MOE) program [28]. The library of analogues was enumerated by attaching the R-groups (fragments, building blocks) onto the APP and AHO scaffolds using the Quasar Combi Design module of MOE program [28]. Chemical reagents considered in this study were taken from the directories of chemicals available from the commercial suppliers of chemicals [29]. Each analogue was built as a neutral molecule in MOE program [28] and its molecular geometry was refined by molecular mechanics optimization using Discovery Studio 2.5 [27] smart minimizer with high convergence criteria (energy difference of 10^{-4} kcal mol^{-1}, R. M. S. displacement of 10^{-5} Å) and a dielectric constant of 4 using class II consistent force field CFF [27] as described in Molecular Mechanics section.

2.9. ADME and Pharmacophore-Based Library Focusing

The library focusing strategy based on ADME-related properties and the pharmacophore-based library focusing procedure is described in ref. [24].

2.10. In Silico Screening

The conformer with the highest mapping (four features) in each cluster was selected for virtual screening using the complexation model. The Gibbs Free Energy (GFE) computed upon E:I complex formation in a solvent was evaluated for each of them to reach the new analogues with favorable pharmacokinetic profile since they were ADMET selected during the first focusing step described in section *§ ADME-based library focusing*. As indicated previously the GFE takes account of many components derived from ideal hydrogen bonds, perturbed ionic interactions, lipophilic inter-actions, contributions, due to the freezing of internal degrees of freedom and due to the loss of translational and rotational entropy of the ligand. The $\Delta\Delta G_{com}$ was then used for prediction of *pf*A-M17 inhibitory potencies (K_i^{pre}) of the focused virtual library of APP and AHO analogues by employing this parameter in a target-specific scoring function. The scoring function, specific for the *pf*A-M17 receptor of *Plasmodium falciparum*: pK_i^{pre} [*pf*A-M17] = a × $\Delta\Delta G_{com}$ + b, was parameterized using the QSAR model described above. The workflow in Figure 3 summarizes the methodology of the Computer Aided Design of AHO analogues molecule.

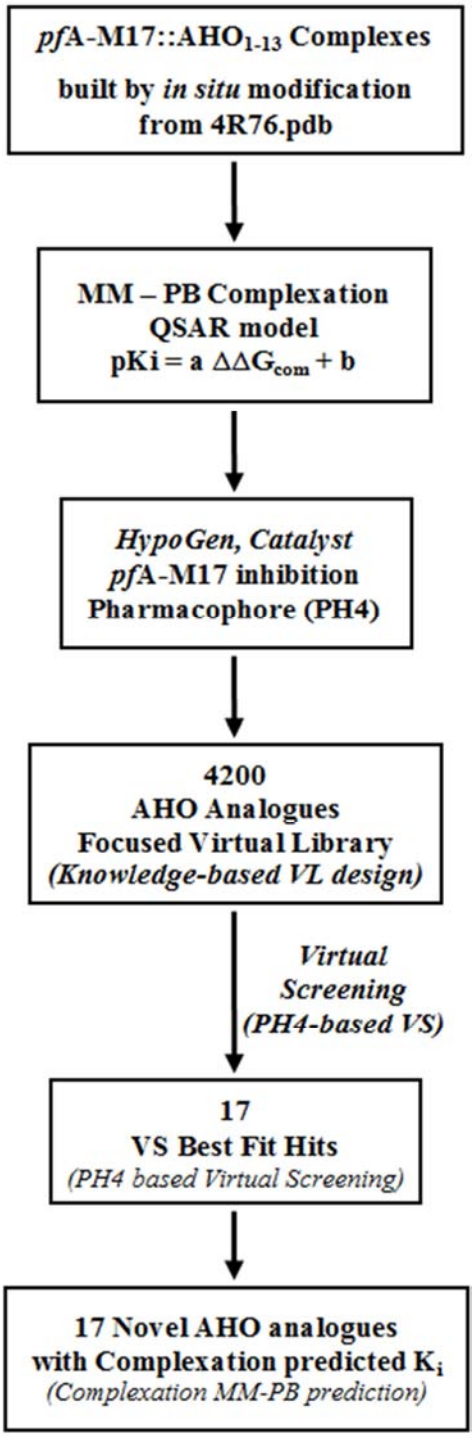

Figure 3. *novel AHO/APP analogues design methodology workflow.*

3. Results and Discussion

A training set of 6 APPs (Table 1) and another of 13 AHOs and validation set of 2 VHOs (Table 2) were selected from a series of compounds with experimentally determined

activities from the same laboratory [12, 13]. Their experimental activities ($11 \leq K_i \leq 1\ 000\ 001$ nM and $8 \leq K_i \leq 501\ 000$ nM respectively) cover sufficiently large range to serve well for building of a reliable QSAR model of *pf*A-M17 inhibition.

3.1. QSAR Models

The relative Gibbs free energy of the enzyme (*E*), inhibitor (I), *E:I* complex formation, equation (6) [24], was computed for the complexes from *in situ* modification of the template inhibitors APP1 and AHO4 respectively in the binding site of *pf*A-M17 as described in the Methods section. Tables 3 and 4 respectively list the $\Delta\Delta G_{com}$ of *E:I* binding and its components, ($\Delta\Delta H_{MM}$, $\Delta\Delta G_{sol}$, $\Delta\Delta TS_{vib}$, $\Delta\Delta G_{com} = \Delta\Delta H_{MM} + \Delta\Delta G_{sol} - \Delta\Delta TS_{vib}$, see equation (6) [24]). At the bottom of each one of both tables the ratio of predicted and observed inhibition constants (pK_i^{pre}/pK_i^{exp}) for the validation set of APPs and AHOs (not included into the training set) are listed. The statistical data of the regression are presented in Figure 4 (A, B and A', B' respectively) and listed in Table 5.

The free energy ($\Delta\Delta G_{com}$) and its enthalpic contribution ($\Delta\Delta H_{MM}$) in tables 3 resp. 4 are computed in an approximate way as indicated in methods section. The relevance of the one descriptor QSAR model derived from these energies is assessed through linear regression correlation with the experimental activity data (K_i). As we can see from table 5 the regression coefficient and Fischer *F*-test values are relatively high indicating a strong correlation between the binding model and the observed inhibitory potencies of the APPs resp. AHOs. The consistency of the model is evaluated through the ratio of predicted and observed inhibition constants (pK_i^{pre} / pK_i^{exp}) for the validation set of AHOs in table 4 (since APPs are in a very short number the whole set totally was reserved for the training set) is close to one confirming the high predictive power of the QSAR models. On the basis of these results, the regression equations and computed $\Delta\Delta G_{com}$ quantities of novel APPs and AHOs analogues, sharing the same binding mode with the training set compounds, can be used to predict their *pf*A-M17 inhibitory concentrations K_i^{pre}.

This Computational approach successfully narrows the filter and accelerates the process to new lead compounds compared with traditional synthesis approach. This was observed for peptide and peptidomimetic inhibitors of HIV-1 [16, 17] and hepatitis C (HCV) [15] virus proteases design, for combinatorial design of bicyclic thymidine analogues [22] and complexation structure-based design of thymidine analogues [21, 23] inhibitors of *Mycobacterium Tuberculosis (MTb*) thymidine monophosphate kinase, to provide insight into selectivity of peptidomimetic inhibitors with modified statine core for *pf* Plasmepsin II over human Cathepsin D [18]. Recently a complete process starting from the complexation QSAR model and its derived 3D-QSAR four features Pharmacophore (PH4) model have successfully served to screen a large Virtual Library of 1.6 million compounds reaching one hundred orally bioavailable pyrrolidine carboxamide inhibitors of *MTb* enoyl acyl carrier protein reductase (InhA) [24].

3.2. Binding Mode of Inhibitors

3.2.1. Free Energy

The binding modes of APPs and AHOs coming from the complexation models are illustrated in 3D depiction in Figure 5 and 6, the last one for the Connolly surface for APP1 and AHO1 respectively. The main interactions at the active sites reported from the reference X-rays structures (Figure 2) are conserved, involving the key residues and S1 and S1' pockets. In order to get a better insight in these interactions, we build the enzyme – inhibitor interaction energy diagram.

3.2.2. Enzyme – Inhibitor Interaction Energy

Besides the complexation enthalpy, entropy and solvation energy, global interaction energy ΔE_{int} can guide in the design of new potent analogues as exemplified by our design of new thymidine analogues [21] where analysis of breakdown of ΔE_{int} into contribution of each active site residue to the interaction with the inhibitor ($\Delta E_{int-ResX}$) shed light on the appropriate substitutions able to improve stabilizing effect of specific residue (ResX) contribution to ΔE_{int} and to affinity *in fine*. In this study, a 40% jump is observed in experimental activity from APP1 (11 nM, the most potent APPs) to AHO1 (8 nM, the best AHOs). Since strong correlation between global interaction energy ΔE_{int} and K_i^{exp} has been noticed as well for APPs (Tables 6) and AHOs (Tables 7) from statistical data in table 8 and the plots in Figure 5, we can try to get insight into ΔE_{int} breakdown ($\Delta E_{int-ResX}$) as provided in table 9 where $\Delta E_{int-ResX}$ are grouped by type of interaction such as H-Bonds ($\Delta E_{int-ResX:HB}$), S1 ($\Delta E_{int-ResX:S1}$) and S1' ($\Delta E_{int-ResX:S1'}$) pockets filling, for the most active inhibitors, APP1 and AHO1 respectively.

For $\Delta E_{int-ResX:HB}$, 17% of E_{int} is HB-based in APP1 versus 25% in AHO1 for a 47% jump closely in the trend of K_i^{exp}.

For $\Delta E_{int-ResX:S1}$, 19% of E_{int} with APP1 versus 15% with AHO1 for a -27% jump, reverse to the trend of K_i^{exp}.

Analysis of table 9 confirms inability of APP1 to reach S1' pocket while AHO1 does. Indeed, for $\Delta E_{int-ResX:S1'}$, about 10% of E_{int} is related to S1' residues' interaction with APP1 while 22% are involved with AHO1 reaching an exaggerated jump of 120%, nevertheless it's in the trend of K_i^{exp}.

In the hypothesis that these three groups of interaction could explain the essentials of interaction between *pf*A-M17 and APP1 and AHO1 respectively, the 46% of E_{int} for APP1 versus 62% for AHO1 corresponds to a 35% jump globally, close to 40% observed experimentally.

On the basis of this result, improvement of interaction with S1 pocket residues as for APPs and with S1' pocket as for AHOs will lead to the design of most active analogues.

4. *pf*A-M17 Inhibition Pharmacophore (PH4) Models

The 3D-QSAR PH4 generation process follows three main steps, the constructive, the subtractive and the optimization steps.

Table 1. *Training set of APP pfA-M17 inhibitors for QSAR model.*

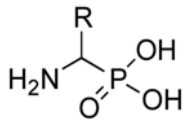

Training Set	R	K_i [nM]
APP 1	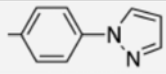	11
APP 2	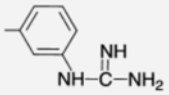	160
APP 3	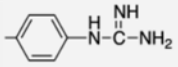	1800
APP 4	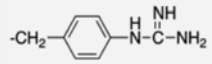	63000
APP 5	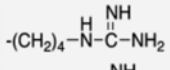	268000
APP 6	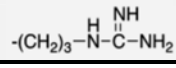	1000001

Table 2. *Training set of AHO inhibitors of pfA-M17 for QSAR model.*

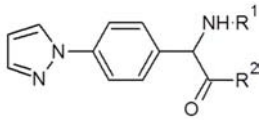

Training Set	R_1	R_2	K_i [nM]
AHO1	2-FluoroBenzoyl	NHOH	8
AHO2	3-FluoroBenzoyl	NHOH	35
AHO3	4-FluoroBenzoyl	NHOH	12
AHO4	3-aminobenzoyl	NHOH	14
AHO5	^{t}Bu (C==O)	NHOH	28
AHO6	^{t}BuNH (C==O)	NHOH	38
AHO7	H. HCl	OH	501000
AHO8	Boc	NHOH	30
AHO9	H. HCl	NHOH	86000
AHO10	Benzoyl	NHOH	154
AHO11	CH_3CH_2 (C==O)	NHOH	16
AHO12	$(CH_3)_2CH$ (C==O)	NHOH	53
AHO13	Boc[a]	OH	464000
VHO1	CH_3 (C==O)	NHOH	19
VHO2	4-aminobenzoyl	NHOH	11

[a]: *tert*-butyloxycarbonyl protecting group.

Table 3. *Complexation energy and its components for the training set of pfA-M17 inhibitors: APP1 – APP6.*

Training Set[a]	M_w[b]	$\Delta\Delta H_{MM}$[c]	$\Delta\Delta G_{sol}$[d]	$\Delta\Delta TS_{vib}$[e]	$\Delta\Delta G_{com}$[f]	K_i^{expg}
APP1	254	0	0	0	0	11
APP2	245	0.27	3.66	0.82	3.11	160
APP3	245	8.70	-2.67	-0.15	6.18	1 800
APP4	259	12.74	-0.78	2.70	9.26	63 000
APP5	255	15.46	-2.42	3.29	9.75	268 000
APP6	211	17.04	-5.07	1.72	10.25	1 000 001

[a] for the chemical structures of the training set of inhibitors see Table 1.
[b] M_w (g mol^{-1}) is the molecular mass of the inhibitor.
[c] $\Delta\Delta H_{MM}$ (kcal mol^{-1}) is the relative enthalpic contribution to the Gibbs free energy change related to the protease-inhibitor complex formation derived by molecular mechanics (MM): $\Delta\Delta H_{MM} \cong [E_{MM}\{PR:AHOx\} - E_{MM}\{AHOx\}] - [E_{MM}\{PR:AHO1\} - E_{MM}\{AHO1\}]$, AHO1 is the reference inhibitor;
[d] $\Delta\Delta G_{solv}$ (kcal mol^{-1}) is the relative solvation Gibbs free energy contribution to the Gibbs free energy (GFE) change related to protease-inhibitor complex formation: $\Delta\Delta G_{solv} = [G_{solv}\{PR:AHOx\} - G_{solv}\{AHOx\}] - [G_{sol}\{PR:AHO1\} - G_{sol}\{AHO1\}]$;
[e] $-\Delta\Delta TS_{vib}$ (kcal mol^{-1}) is the relative entropic contribution of the inhibitor to the GFE related to protease-inhibitor complex formation: $\Delta\Delta TS_{vib} = [TS_{vib}\{AHOx\}_{PR} - TS_{vib}\{AHOx\}] - [TS_{vib}\{AHO1\}_{PR} - TS_{vib}\{AHO1\}]$;
[f] $\Delta\Delta G_{comp}$ (kcal mol^{-1}) is the relative GFE change related to the enzyme-inhibitor complex formation: $\Delta\Delta G_{comp} \cong \Delta\Delta H_{MM} + \Delta\Delta G_{solv} - \Delta\Delta TS_{vib}$.
[g] K_i^{exp} (nM) is the experimental *pf*A-M17 inhibition constant from ref. [12].

Table 4. *Complexation energy and its components for the training set of pfA-M17 inhibitors: AHO1 – AHO13.*

Training Set[a]	M_w[b]	$\Delta\Delta H_{MM}$[c]	$\Delta\Delta G_{sol}$[d]	$\Delta\Delta TS_{vib}$[e]	$\Delta\Delta G_{com}$[f]	K_i^{expg}
AHO1	354	0	0	0	0	8
AHO2	354	-0.20	0.80	0.01	0.59	35
AHO3	354	-0.01	1.98	-0.11	2.08	12
AHO4	351	0.07	1.07	1.91	-0.77	14
AHO5	316	6.51	-0.55	4.41	1.55	28
AHO6	331	7.91	0.57	5.14	3.34	38
AHO7	216	29.19	1.26	3.98	26.47	501000
AHO8	332	4.41	1.42	4.30	1.53	30
AHO9	232	30.84	-5.40	4.57	20.87	86000
AHO10	334	3.35	7.07	0.98	9.44	154
AHO11	288	7.35	-1.24	3.19	2.92	16
AHO12	302	8.12	-2.83	0.69	4.60	53
AHO13	316	22.58	9.25	2.09	29.74	464000

Validation Set	M_w	$\Delta\Delta H_{MM}$	$\Delta\Delta G_{sol}$	$\Delta\Delta TS_{vib}$	$\Delta\Delta G_{comp}$	pK_i^{pre}/pK_i^{exp}[h]
VHO1	274	8.86	-1.78	2.64	4.44	0.94
VHO2	351	1.42	1.24	1.97	0.69	0.99

[a – f] (see Table 3 with "APP" changed into "AHO"). For the chemical structures of the training set of inhibitors see Table 2.
[g] K_i^{exp} (nM) is the experimental *pf*A-M17 inhibition constant from ref. [13].
[h] ratio of predicted and experimental inhibition constants pK_i^{pre}/pK_i^{exp}. K_i^{pre} was predicted from computed $\Delta\Delta G_{com}$ using the regression equation (D) for *pf*A-M17 shown in Table 5.

Table 5. *Statistical information on regression analysis of correlation for the training set between $\Delta\Delta H_{MM}$, $\Delta\Delta G_{com}$ and experimental activities (K_i^{exp}) respectively against pfA-M17, (A), (B) for APPs and (C), (D) for AHOs.*

$pK_i^{exp} = -0.2552 \cdot \Delta\Delta H_{MM} + 7.5181$	(A)
$pK_i^{exp} = -0.4626 \cdot \Delta\Delta G_{com} + 8.1842$	(B)
$pK_i^{exp} = -0.1523 \cdot \Delta\Delta H_{MM} + 8.0541$	(C)
$pK_i^{exp} = -0.1665 \cdot \Delta\Delta G_{com} + 7.9581$	(D)

Statistical data of regression	**(A)**	**(B)**	**(C)**	**(D)**
Number of compounds n	6	6	13	13
Squared regression correlation coefficient R^2	0.96	0.98	0.88	0.97
LOO cross-validated squared correlation coefficient $R_{XV}{}^2$	0.95	0.97	0.85	0.96
Standard error of the regression σ	0.956	0.279	0.658	0.305
Statistical significance of regression, Fisher F-test *F*	109.4	238.8	78.2	403.4
Level of statistical significance α	> 95%	> 95%	> 95%	> 95%
Range of activity K_i^{exp} (nM)	11 – 1000001		8 - 501000	

The constructive phase of HypoGen automatically selected as leads the most active compounds for which ($K_i^{exp} \times 1.25 - K_i^{exp}/1.25 > 0$). For AHOs, only AHO1, $8 \times 1.25 - K_i^{exp}/1.25 > 0$ or $K_i^{exp} < 12.5$, was retained as lead. In the same way, for APPs, $K_i^{exp} < 17.2$, only APP1 was retained as lead. Both APP1 and AHO1 were used to generate all starting PH4 features respectively. Only those were retained which matched respectively both leads APP1 and AHO1.

In the subtractive phase inactive compounds with $\log_{10}(K_i^{exp}) - \log_{10}(K_i^{exp}) > 3.5$ were used to remove those pharmacophoric features that mapped more than 50% of these compounds while pharmacophore representatives which contained all features were retained. APP4, 5 and 6 were used to remove from $PH4_{APP}$ the features mapping > 50% of them while AHO7, 9 and 13 served to remove from $PH4_{AHO}$ the features mapping > 50% of them as well.

In the optimization phase, the highest scoring PH4s according to their probability function cost calculated based on a simulated annealing algorithm, were retained. A total of 10 optimized hypotheses were kept all displaying four features for each pharmacophore.

The features, their internal coordinates and their mapping are displayed in Figure 8 (A, A' and B, B' respectively). The statistical data for the set of hypotheses (costs, RMSD, R) are listed in Tables 10 (for APP) and 11 (for AHO) for both PH4, while the statistical information on regression analysis correlation for the training set between estimated activities and experimental ones are listed in table 12.

The bound conformation of inhibitors at *pf*A-M17 active site reveals a great deal of information about affinity. The best way of exploiting them consists in generating the Pharmacophore (PH4) of activity. The process is described in the methods section. The reliability of the generated pharmacophore models was then assessed through the calculated cost parameters. As indicated in tables 10 and 11 for APPs resp. AHOs the overall costs ranged from 41.2 (Hypo1) to 48.2 (Hypo10) for APPs and from 492.1 (Hypo1) to 854.7 (Hypo10) for AHOs. The gap between the highest and lowest cost parameter was relatively small and matched well with the homogeneity of the generated hypotheses and the consistency of the training set. For the best APPs' PH4 model the fixed cost (26.3) was lower than the null cost (741.1) by Δ = 714.8; in the same way the best AHOs' PH4 model fixed cost (23.4) was lower than the null cost (11552.9) by Δ = 11529.5. This difference represents a chief indicator of the predictability of the PH4 model (Δ > 70 corresponds to a probability higher than 90% that the model represents a valid correlation [21]). In order to be statistically significant the hypotheses have to reach values as close as possible to the fixed cost and as far as possible from the null cost.

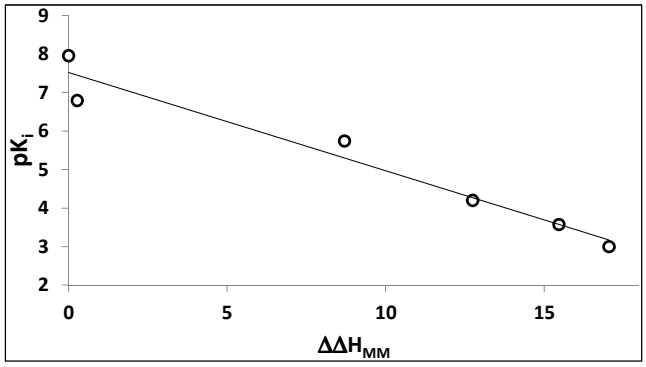

(A)

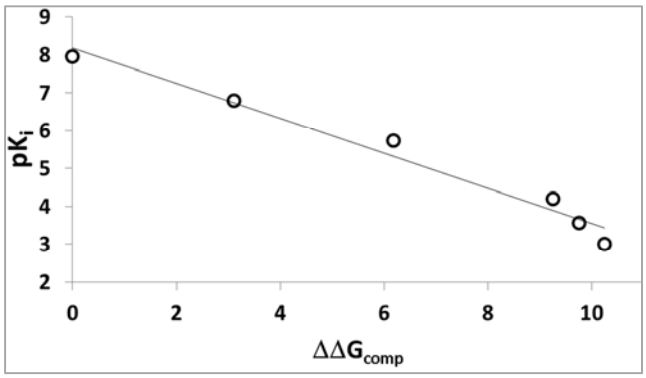

(B)

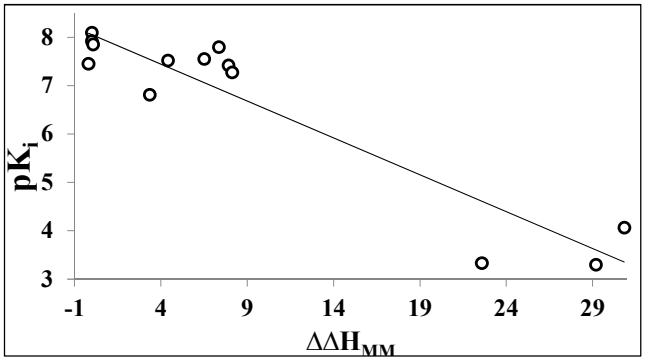

(A')

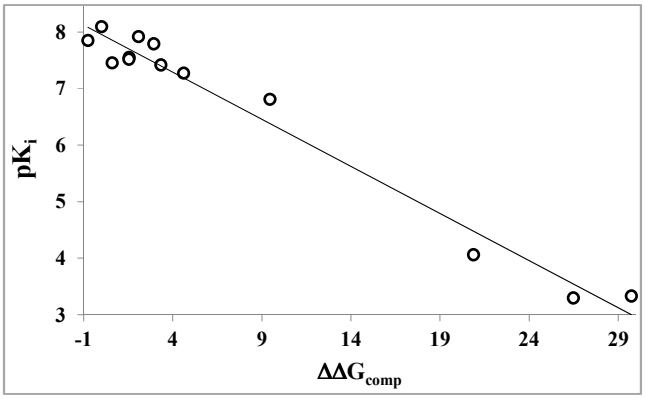

(B')

Figure 4. *QSAR models of APP (A, B) and AHO (A', B') respectively.*

The differences $\Delta \geq 699.9$ for the set of 10 APPs' PH4 hypotheses and $\Delta \geq 11060.8$ for the set of 10 AHOs' PH4 hypotheses confirm the high quality of the pharmacophore models $PH4_{APP}$ and $PH4_{AHO}$. Standard indicators such as the root-mean-square deviation (RMSD) between the hypotheses ranged from 1.009 to 1.709 for APPs and from 8.351 to 10.692 for AHOs while the squared correlation coefficient (R^2) occupied an interval from 0.998 to 0.994 for APPs and from 0.98 to 0.96 for AHOs. The PH4 hypothesis with the best RMSD and highest R^2 for APPs and for AHOs respectively was retained for further analysis; they have been selected from the detailed statistical data for the set of hypotheses (costs, RMSD, R^2) and listed in Tables 10 resp. 11. The geometries of the Hypo1 pharmacophore of *pf*A-M17 inhibition are displayed on Figure 8 for APPs (A) and AHOs (A'): features and coordinates between them for each APPs' and AHOs' PH4 respectively and with the best inhibitor APP1 and AHO1 mapped to them. Clearly both PH4 are different from each other and not superimposable: $PH4_{APP}$ featuring S1 pocket filling while $PH4_{AHO}$ targets S1 and S1' filling as exemplified by Figure 9. The consistency of the model is reinforced by the position of the $PH4_{APP}$ with APP1 resp. $PH4_{AHO}$ with AHO1 mapped to it at the enzyme active site as displayed in Figure 10. From this the mapping to the PH4s gives a reliable indication of the level of enzyme – ligand affinity at the *pf*A-M17 active site.

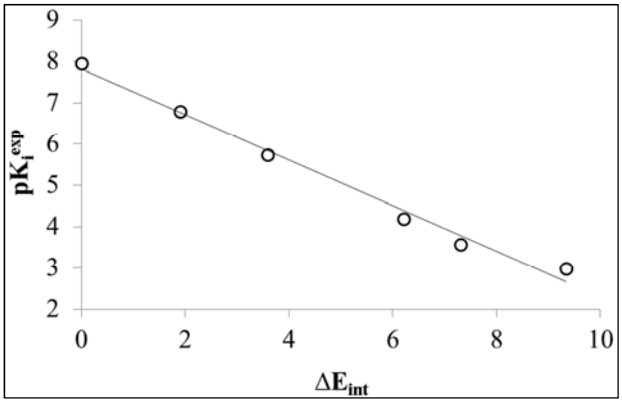

(A)

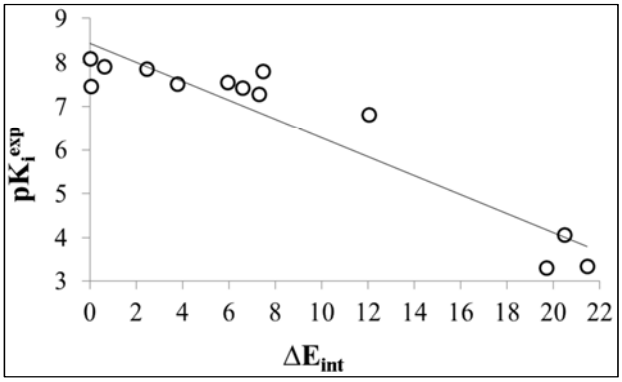

(B)

Figure 5. *Global Enzyme – ligand interactions energy (E_{int}) regression plots for APP (A) and AHO (B) respectively.*

Table 6. *Global Enzyme – ligand (PR:APP1) interactions energy (E_{int}) for the training set of pfA-M17 inhibitors: APP1 – APP6.*

Training Set[a]	ΔE_{int} [a]
APP1	0
APP2	1.9
APP3	3.6
APP4	6.2
APP5	7.3
APP6	9.3

[a]ΔE_{int} (kcal.mol^{-1}) is the interaction energy as defined in Methods section: $\Delta E_{int} = E_{int}${PR:APPx}-E_{int}{ PR:APP1}, APP1 is the reference inhibitor.

Table 12 lists the regression equations for pK_i^{exp} vs. pK_i^{pre} estimated from Hypo1 for APPs (A) and AHOs (B) along with related indicators such as R^2, R_{xv}^2, F-test and σ with α > 95% while Figure 8 (B and B') displays their plot respectively for APPs and AHOs. For the AHOs validation set the ratio pK_i^{pre}/pK_i^{exp} has been computed for VHO1:1.03 and VHO2:1.04 both relatively close to one which attests the substantial predictive power of this regression for the best PH4 model. The selected PH4 models will serve in virtual screening of APPs and AHOs designed analogues libraries.

5. New *pf*A-M17 APP and AHO Inhibitors Analogues

The diversity library design of new APP and AHO

analogues inhibitors of *pfA-M17* was based on substitutions at one position for APP (in order to better fit S1 pocket at the enzyme active site) and two for AHO (in order to better fit S1 and S1' pockets). The 77 and 134 R-groups used are listed in tables 13 and 16 for APP and AHO respectively.

Table 7. *Global Enzyme – ligand (PR:AHOx) interactions energy (E_{int}) for the training set of pfA-M17 inhibitors: AHO1 – AHO13.*

Training Set[a]	ΔEint[a]
AHO1	0
AHO2	0.1
AHO3	0.6
AHO4	2.4
AHO5	5.9
AHO6	6.6
AHO7	19.7
AHO8	0.9
AHO9	20.5
AHO10	12.0
AHO11	7.4
AHO12	7.3
AHO13	21.4

Validation Set	$pK_i^{pre}/pK_i^{exp\ b}$
VHO1	0.87
VHO2	1.03

[a]ΔE_{int} (kcal.mol^{-1}) is the interaction energy as defined in Methods section: $\Delta E_{int} = E_{int}${PR:AHOx}-E_{int}{PR:AHO1}, AHO1 is the reference inhibitor;
[b]ratio of predicted and experimental inhibition constants pK_i^{pre}/pK_i^{exp}. K_i^{pre} was predicted from computed ΔE_{int} using the regression equation (B) for *pf*A-M17 shown in Table 8.

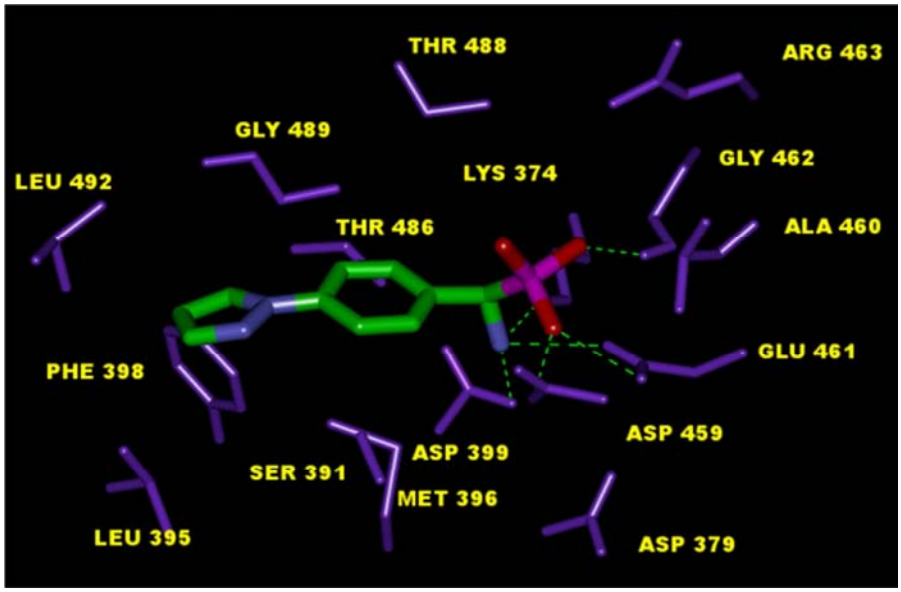

(A)

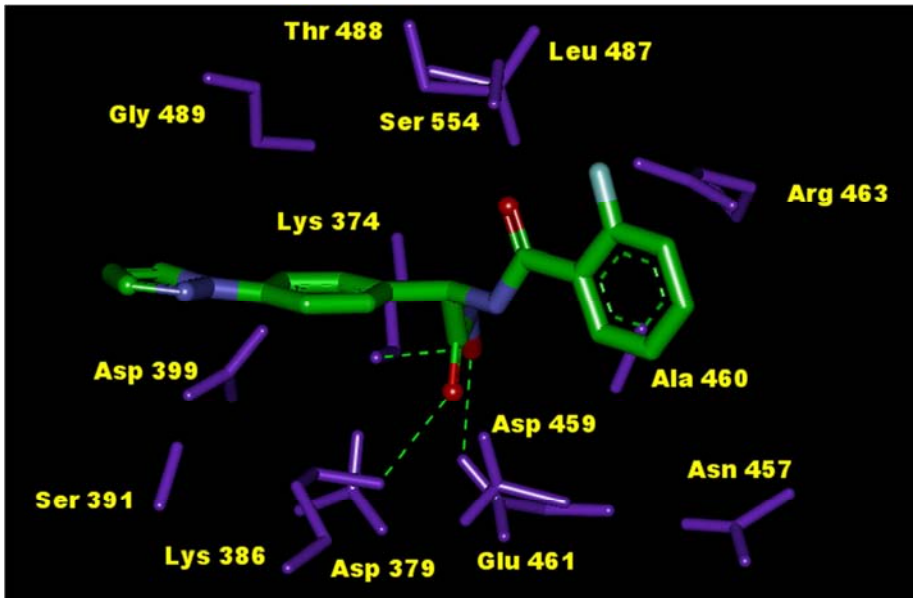

(B)

Figure 6. *Enzyme – ligand interactions at the active site of pfA-M17 depicted in 3D for the most active APP (A) namely APP1, AHO (B), AHO1 respectively.*

Table 8. *Statistical data on regression analysis of correlation for the APP (A) and AHO (B) training sets between ΔE_{int} and pfA-M17 inhibition experimental activities (K_i^{exp}).*

$pK_i^{exp} = -0.5514 \cdot \Delta E_{int} - 19.89$	(A)
$pK_i^{exp} = -0.2142 \cdot \Delta E_{int} - 4.76$	(B)

Statistical data of regression	**(A)**	**(B)**
Number of compounds n	6	13
Squared correlation coefficient of regression R^2	0.99	0.88
LOO cross-validated squared correlation coefficient R^2_{XV}	0.98	0.87
Standard error of the regression σ	0.24	0.6521
Statistical significance of regression, Fisher F-test *F*	337.8	81.978
Level of statistical significance α	> 95%	> 95%
Range of activity of K_i^{exp} (nM)	11 – 1000001	8 - 501000

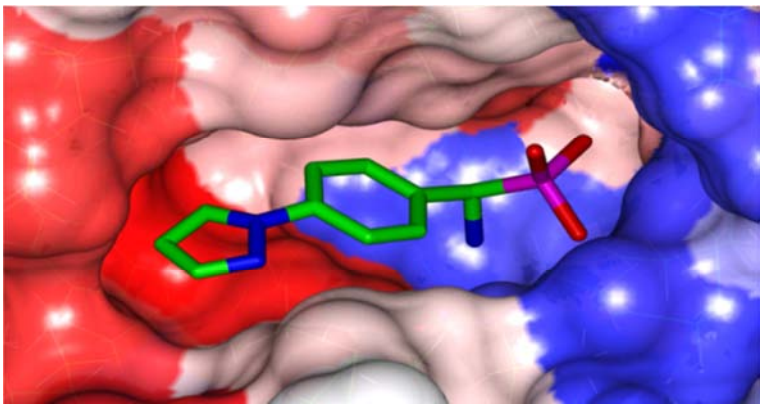

(A)

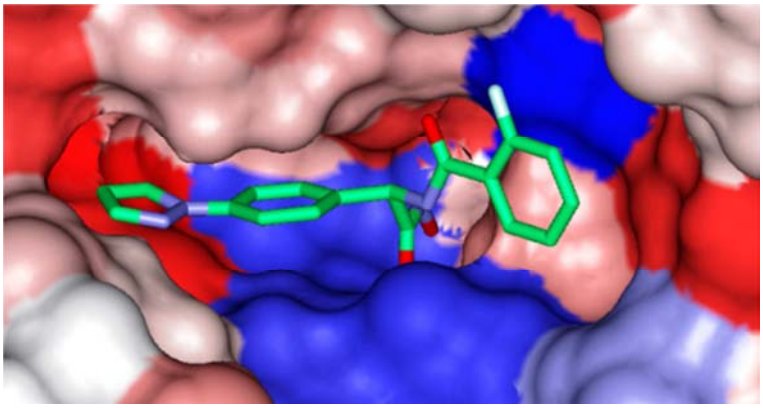

(B)

Figure 7. *Connolly surface of pfA-M17 active-site with bound most active APP (A) namely APP1, AHO (B), AHO1 inhibitor respectively. The binding site surface is colored according to residue hydrophobicity: red – hydrophobic, blue – hydrophilic, and white – intermediate.*

Table 9. *Breakdown of pfA-M17 global interaction energy to each active site residue contribution for H-Bonds, S1 and S1' pockets in the case of the most active inhibitors, APP1 and AHO1 respectively.*

(% of E_{int})	***pf*A-M17:APP1 (A)**	***pf*A-M17:AHO1 (B)**
H-BOND	Lys374 – 12%	–
	–	Asp379 – 5%
	Lys386 – 3%	Lys386 – 5%
	Asp399 – 2%	Asp459 – 8%
	–	Leu487 – 6%
	17% of total E_{int}	25% of total E_{int}
S1 pocket	Met392 – 1%	Met392 – 1%
	Met396 – 6%	Met396 – 3%
	Phe398 – 3%	Phe398 – 2%
	Gly489 – 4%	Gly489 – 5%
	Tyr493 – 2%	Ala577 – 2%
	Ala577 – 3%	Tyr493 – 2%

(% of E_{int})	*pf*A-M17:APP1 (A)	*pf*A-M17:AHO1 (B)
	19% of total E_{int}	**15% of total E_{int}**
	Arg463 – 4%	Arg463 – 6%
	Ile547 – 0.1%	Ile547 – 2%
	Ala460 – 5%	Ala460 – 5%
S1' pocket	Asn457 – 0.1%	Asn457 – 3%
	Ser554 – 0.1%	Ser554 – 4%
	Lys552 – 0.5%	Lys552 – 2%
	9.8% of total E_{int}	**22% of total E_{int}**

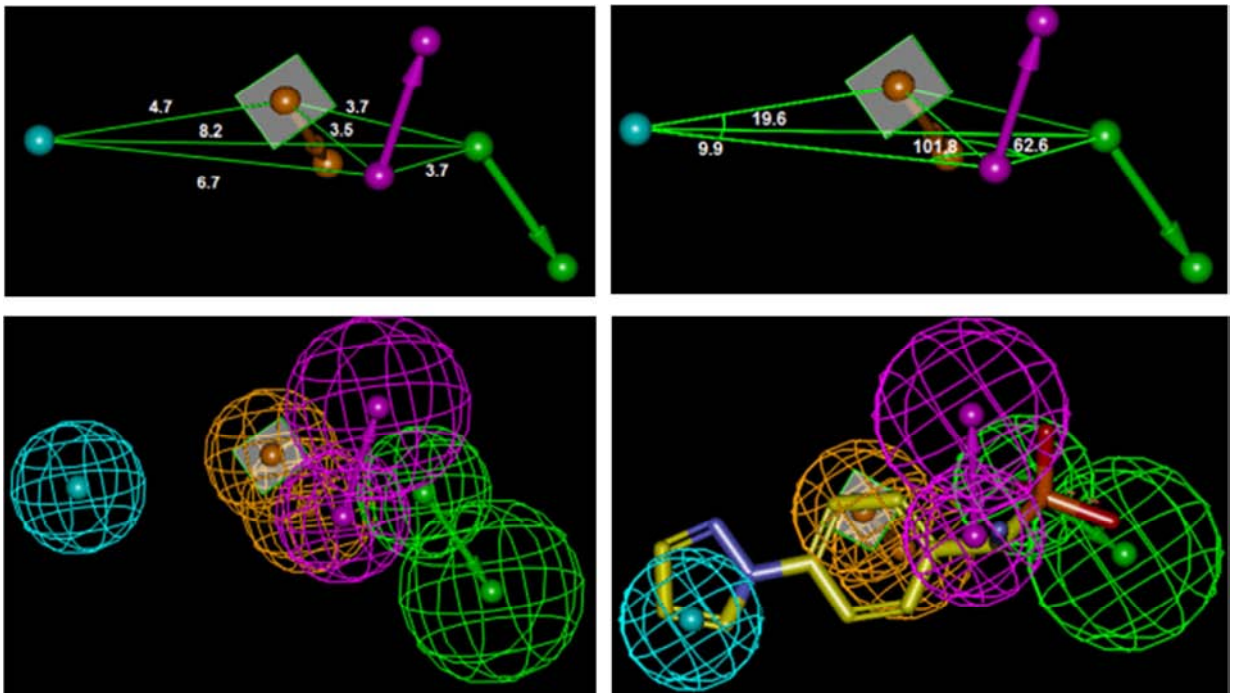

(A)

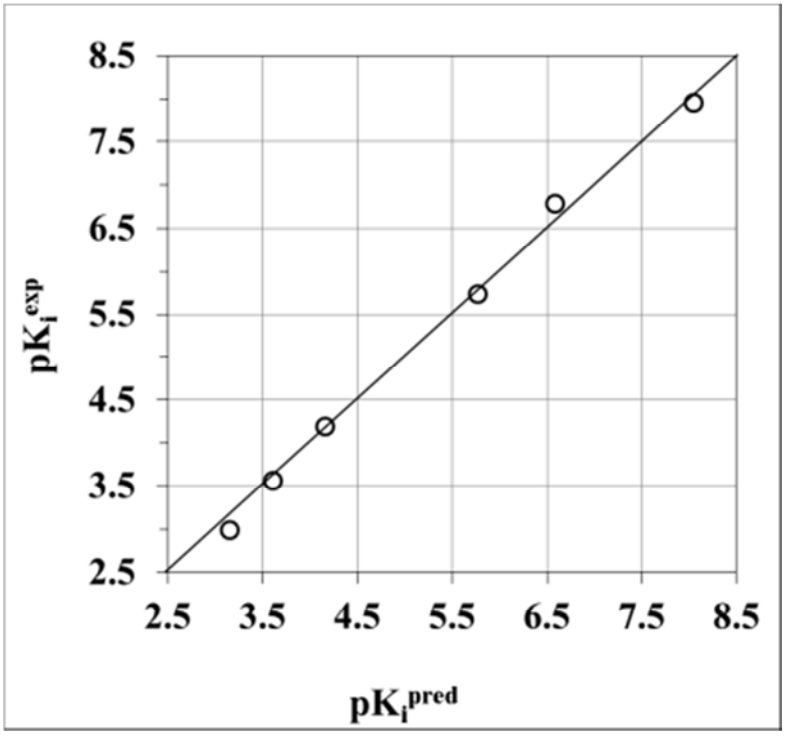

(B) APP

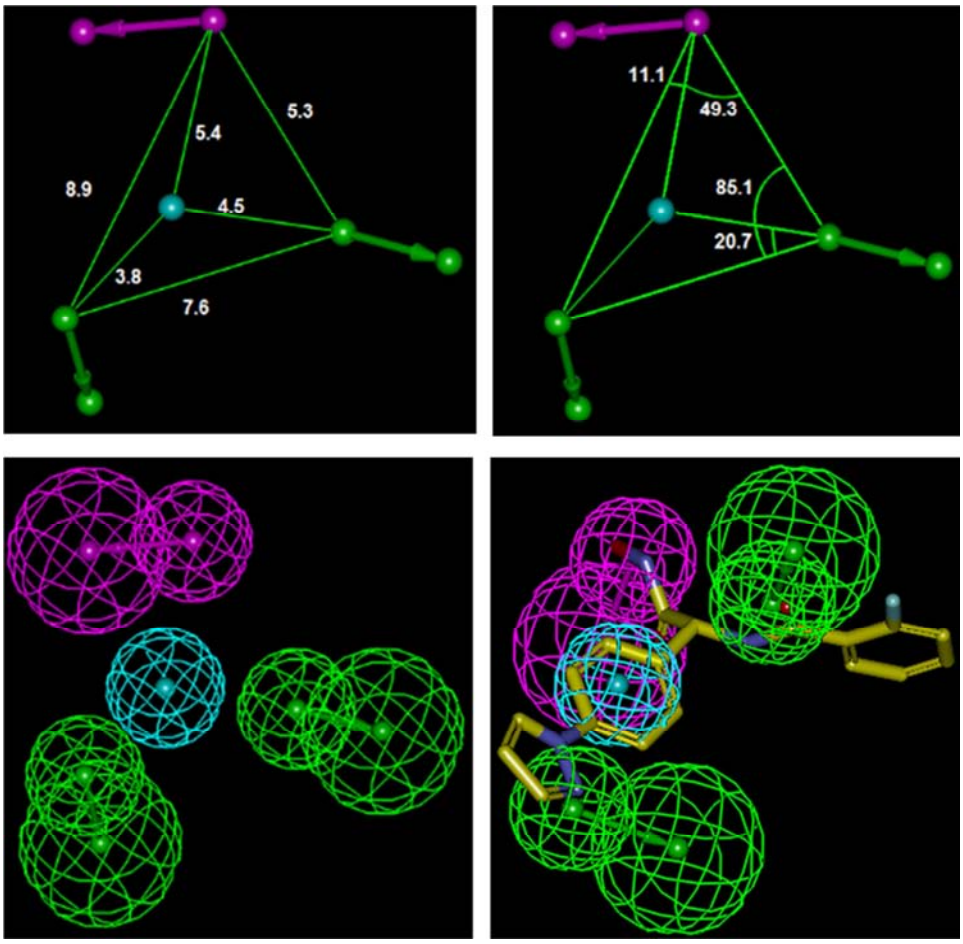

(A')

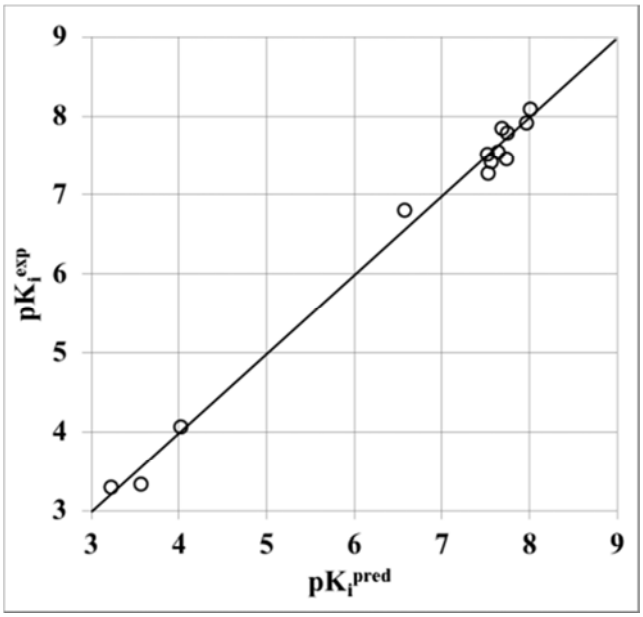

(B') AHO

Figure 8. *Pharmacophore (PH4) models of APP (A, B) and AHO (A', B') respectively displaying: the features and their internal coordinates (distances and angles), mapping of APP1 and AHO1 to each respective pharmacophore (A, A') and the plot of estimated and experimental activity for each PH4 (B, B').*

Table 10. *Output parameters of the 10 generated PH4 Hypotheses for APPx after CatScramble validation procedure for pfA-M17 inhibitors listing RMSD, total cost and R correlation coefficient.*

Hypothesis	RMSD	R^2	Total costs
Hypo1	1.009	0.998	41.2
Hypo 2	1.474	0.995	43.1
Hypo 3	1.731	0.993	44.1
Hypo 4	1.644	0.994	44.8
Hypo 5	1.841	0.993	44.8
Hypo 6	1.612	0.994	44.9
Hypo 7	1.597	0.994	45.3
Hypo 8	1.889	0.992	46.3
Hypo 9	1.587	0.995	47.1
Hypo 10	1.709	0.994	48.2
Fixed cost	0	1.0	26.3
Null cost	15.594	0	741.1

Table 11. *Output parameters of the 10 generated PH4 Hypotheses for AHOx after CatScramble validation procedure for pfA-M17 inhibitors listing RMSD, total cost and R correlation coefficient.*

Hypothesis	RMSD	R^2	Total costs
Hypo1	8.351	0.98	492.1
Hypo 2	8.391	0.97	497.3
Hypo 3	8.745	0.97	546.3
Hypo 4	9.169	0.97	585.6
Hypo 5	9.169	0.97	585.6
Hypo 6	9.158	0.97	589.3
Hypo 7	10.186	0.97	722.0
Hypo 8	10.522	0.96	778.2
Hypo 9	10.632	0.96	793.0
Hypo 10	10.692	0.96	854.7
Fixed cost	0	1.0	23.4
Null cost	42.137	0	11552.9

Table 12. *Statistical information on regression analysis of correlation for the training set between PH4 predicted activity (pKi^{pred}) and experimental one (pKi^{exp}) for APP (A) and AHO (B) respectively against pfA-M17.*

$pK_i^{exp} = 1.02016 \cdot pK_i^{pred} - 0.10478$	(A)
$pK_i^{exp} = 0.99677 \cdot pK_i^{pred} - 0.00457$	(B)

Statistical data of regression	(A)	(B)
Number of compounds n	6	13
Squared correlation coefficient of regression R^2	0.99	0.99
LOO cross-validated squared correlation coefficient R^2_{XV}	0.99	0.98
Standard error of the regression σ	0.1342	0.1707
Statistical significance of regression, Fisher F-test *F*	1047.8	1312.9
Level of statistical significance α	> 95%	> 95%
Range of activity of K_i^{exp} (nM)	11 – 1000001	8 - 501000

5.1. Library Design

In order to identify more potent orally bioavailable *pf*A-M17 inhibitors we have built two virtual libraries; first for new APP with a variety of substitutions in one position, second for new AHO with substitutions in two positions. During the virtual library enumeration the R-groups listed in Table 13 were attached to position R_1 for APPs of the appropriate scaffold to form a combinatorial library of the size: 77 APP analogues. In the same way R_1 and R_2 positions of AHOs have been substituted with R-groups from Table 16, $R_1 \times R_2 = 84 \times 50 = 4{,}200$ AHO analogues. All analogues are matching the substitution pattern of the best inhibitor APP1 and AHO1 respectively.

These diversity libraries of APPs and AHOs analogues were generated from the substituted phosphonic arginine and hydroxamic acids listed in the databases of available chemicals [29]. Nowadays one of the criteria for the design of new antimalarials, in regards to the target population, is their oral bioavailability. In order to design a more focused library of a reduced size and increased content of drug-like and orally bioavailable molecules, we have introduced a set of filters and penalties, which can help to select smaller number of suitable APPs and AHOs that can be submitted to *in silico* screening. The initial virtual library was thus filtered in an ADME-based focusing step to remove compounds with expected poor oral bioavailability and low drug likeness. For AHOs only analogues with high predicted percentage of human oral absorption (HOA) in the gastrointestinal tract larger than 25% (25% is the highest value of poor oral bioavailability compounds, see legend [(r)] in table 20) [24] and compounds satisfying the Lipinski's rule of five [30] computed for the

entire virtual library using QikProp software [14], were kept. Let's recall that this focusing was not applied for APPs analogues since they were used here to guide S1 pocket interaction improvement only, their ADME profile is already known to be not favorable as table 20 confirms for most of them.

5.2. In Silico Screening of Libraries of APPs and AHOs

The libraries of APPs and AHOs analogues were further screened for molecular structures matching to the 3D-QSAR PH4 pharmacophore model Hypo1 of *pf*A-M17 inhibition by APPs ($PH4_{APP}$) and AHOs ($PH4_{AHO}$) respectively.

5.2.1. Library of APPs

From the set of 77 analogues, only 16 best fitting analogues ($PH4_{APP}$ hits) have been retained and submitted to screening with help of the complexation QSAR model. Computed Gibbs free energy upon complex formation with *pf*A-M17 and its components as well as predicted K_i^{pre} estimated from the correlation Equation (B), table 5, are given in table 14. For a short majority of new APP analogues, the estimated inhibitory potencies shown in Table 14 are better than that for the most active training set compound APP1 (K_i^{exp} = 11 nM [12]).

The main goal of the design of APP analogues is to provide structural information, essentially appropriate substituent sup-posed to serve in discovery of new scaffold or to improve existing one such as AHOs' affinity.

5.2.2. Library of AHOs

From the set of 4200 analogues of AHOs 4128 mapped to at least 2 features, 3615 of which mapped to 4 features of the pharmacophore. Out of then, only 17 best fitting analogues (PH4 hits) have been retained and submitted to screening with help of the complexation QSAR model. Computed Gibbs free energy of complex formation with *pf* A-M17 and its component as well as predicted K_i^{pre} estimated from the correlation Equation (D), table 5, are given in tables 17 and 18. For a majority of new AHO analogues, the estimated inhibitory potencies shown in table 17 are better than that for the most active training set compound AHO1 (K_i^{exp} = 8 nM [13]).

5.3. Analysis of New Inhibitors

In order to identify which substituents on the APPs (Table 13) lead to new inhibitor candidates with the highest predicted potencies against *pf*A-M17, we have analyzed the frequency of occurrence of R_1, groups in the APPs and R_1, R_2 groups in the AHOs PH4 best fitting hit selected from the focused virtual library shown in tables 15 and 18.

For the 16 selected APPs the following R-groups were present: 1, 2, 6, 20, 23, 30, 32, 43, 44, 50, 58, 59, 60, 61, 73 and 76; those in top ranked analogues (K_i^{pred} < 1 nM) are 30, 43, 44 and 61; they fill the S1 pocket better. In fact, for the best-designed APP analogue APP-A-43 the predicted K_i is more than 73 times higher than for the APP1 based on a better fitting of the 4-(1H-pyrazol-1-yl)phenyl group in S1 hydrophobic pocket with a sensitivity to the additional methyl group orientation (see also APP-A-44).

For the 17 selected AHOs in R_1 position 14 R-groups are presents once: 6, 7, 10, 12, 24, 26, 44, 47, 50, 54, 74, 77, 81 and 82 except 10 and 44 present twice for fitting S1' pocket. R_2 position (for S1 pocket filling) is less spread since 10 R-groups are presents once: 93, 95, 112, 116, 118, 125 and 133 while 92 and 108 twice and 127 five times among them the best AHO new analogue A-81-127. A-10-112 analogue keeping the methyl extended 4-(1H-pyrazol-1-yl) phenyl group in S1 (as suggested from APPs best analogue) reached a predicted potency of 3.7 nM, in other words, twice more potent than AHO1. In order to improve better the potency, a larger R-group (#127) fitted better in S1 pocket while a CF_3-phenyl occupies S1' pocket to reach the best-designed AHO analogue A-81-127 displaying a predicted inhibitory potency more than 40 times higher than for the AHO1.

Figure 11 displays interactions of best designed APP (A) and AHO (B) analogues respectively with *pf*A-M17. As one can see, besides S1 and S1' pockets hydrophobic contacts, Hydrogen Bonds were conserved. In Figure 12, the AHO analogue (B) fits better in S1 and S1' pockets than the best active training set AHO1 (see Figure 6 and 7, B) justifying, in a large part, the predicted increase of inhibitory potency of A-81-127. Specifically in Figure 11 (B), the hydrogen bond contact involving the ligand and Tyr 493 specific to *pf*A-M17 (in the human ortholog *h*A-M17, it's a Valine residue) may be exploited to enhance the selectivity of A-81-127 as suggested by E. Cunningham et al. [7].

6. ADME Profiles of Designed APPs and AHOs

Two main requirements from WHO about new antimalarials is their low cost and oral bioavailability. About this last one; table 19 displays ADME profile of predicted best active APP analogues. As expected their%$HOA^{(r)}$ are lower than 32%. The range for 95% of drugs (< 25% - poor, > 80% high) clearly indicates almost poor oral bioavailability. In the same way, predicted apparent Caco-2 cell membrane permeability in Boehringer-Ingelheim scale, for which the range for 95% of drugs (< 25 poor, > 500 great) $^{(n)}$ in table 19 confirms their poor membrane permeability as indicated formerly [13]. Let's recall that APPs served to get insight into S1 pocket impact for affinity improvement. Oppositely, as indicated in Table 20, AHOs ADME profile for the best designed new analogues displays%HOA in a higher range for their majority. Only one of them, the less active in this short list, displays poor cell membrane permeability. For almost all of them drug likeness defined as the number of stars, namely the number of property descriptors (from 24 out of the full list of 49 descriptors of QikProp, ver. 3.7, release [14]) that fall outside of the range of values for 95% of known drugs, equals 0. For comparison purpose, the computed ADME profile of some current antimalarials is displayed at the bottom of table 19. As we can see, for almost all antimalarials of the Artemisinin Combined Therapy (ACT) initiative the number of stars is greater than 0 despite their high%HOA.

7. Conclusions

The studied enzyme *pf*A-M17 active site pockets S1 and S1' have been investigated separately as reported through various papers. The hydrophobic S1 suitably accommodates hPhe [31] while the larger amphipathic S1'pocket with hydrophilic neck and hydrophobic extended cavity was expected to improve the target inhibition [13]. Fitting R-group in S1' remained one of the main goals of this work. Accordingly our unrestrained effort to retrieve structural information from the crystal structure of *pf*A-M17 – APP1 and *pf*A-M17 – AHO1 complexes in order to elaborate reliable one descriptor QSAR models of *pf*A-M17 inhibition for APPs and AHOs inhibitors using training and validation sets with known inhibitory activities [12, 13]. The unique descriptor, namely the computed Gibbs free energies (GFE) upon complex formation, correlated with observed inhibitory potencies. Since GFE is a combined descriptor involving enthalpic gas phase, solvation free energy and entropic contributions, a precise and deeper insight into S1 and S1' pockets filling have been retrieved from the model. A consistent way to crosscheck this structural information was the analysis of interactions between the enzyme active-site residues and the inhibitor. In this regard the breakdown of interaction energy to each active site residue contribution clearly ordered the pockets S1' >> S1 when comparing their affinity with APP1 and AHO1: a key information (Table 9) which directed our effort to design an initial diversity virtual combinatorial library of new analogues to be screened by the pharmacophore models derived from the GFE QSAR. The initial library filtered by a set of ADME-related descriptors to a focused one subsequently was screened by mapping of the analogues to the $PH4_{AHO}$ pharmacophore to reach a selected library subset of potent and orally bioavailable AHOs. This subset of 17 best virtual hits was submitted to the computation of predicted *pf*A-M17 inhibitory potencies by the formerly elaborated complexation $QSAR_{AHO}$ model. Starting from a training set led by AHO1 (K_i^{exp}=8 nM), our best designed analogues reached predicted K_i in the low nanomolar concentration range. The best designed AHOs analogues A.50.108 (K_i^{pre} = 0.4 nM), A-81-127 (K_i^{pre} = 0.2 nM), A-7-127 (K_i^{pre} = 0.4 nM) and A-44-92 (K_i^{pre} = 0.3 nM), see tables 17 and 18, are recommended for synthesis and subsequent activity evaluation in *pf*A-M17 inhibition assays and may lead to a discovery of novel potent orally bioavailable lethal and selective antimalarials.

Since *pf*A-M17 is a recent target the inhibition of which is at the beginning era, besides the list of 17 best virtual hits, the Structure Activity Relationship (SAR) information we provide about non potent analogues namely the non-suitable R-groups is of interest for medicinal chemists since they will know the analogues that are not worth synthesizing. More detailed such information is available on demand.

At the end *pf*A-M17 S1 and S1' pockets have to be targeted synergistically: while fitting S1' to improve affinity with *pf*A-M17 better than S1, the latter subsite, through hydrogen bonding the selective enzyme residue Tyr 493 keeps the inhibitor selective over human *h*A-M17 as exemplified by our best designed A-81-127.

Conflict of Interest

"The author (s) declare (s) that there is no conflict of interest regarding the publication of this manuscript."

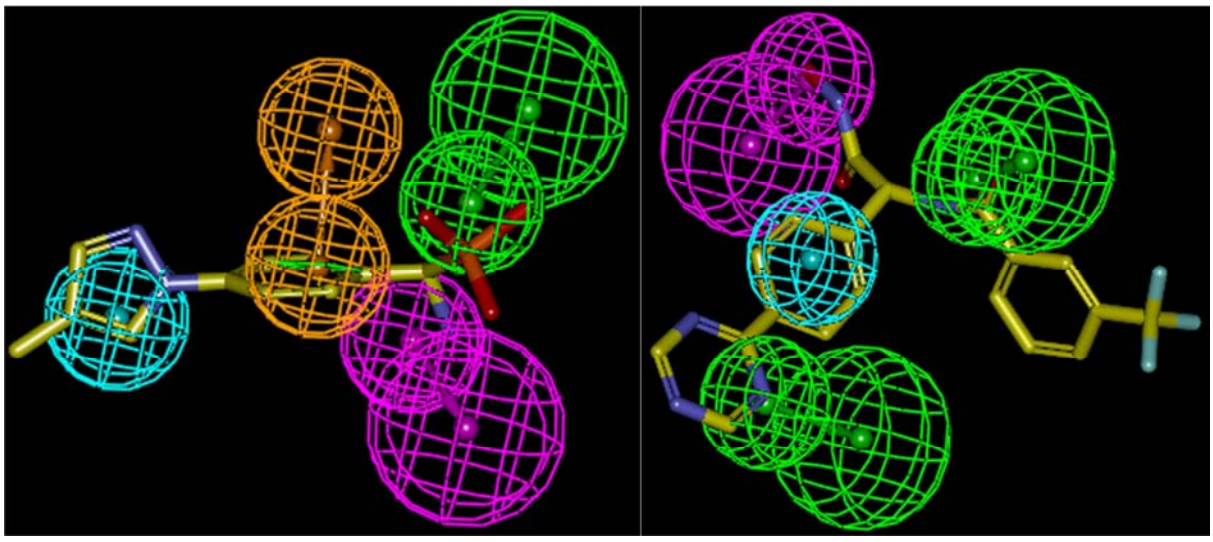

Figure 9. *Best APP designed analogue (APP-A-43) mapped to APP – PH4 (left) and best AHO designed analogue (A-81-127) mapped to AHO – PH4 (right).*

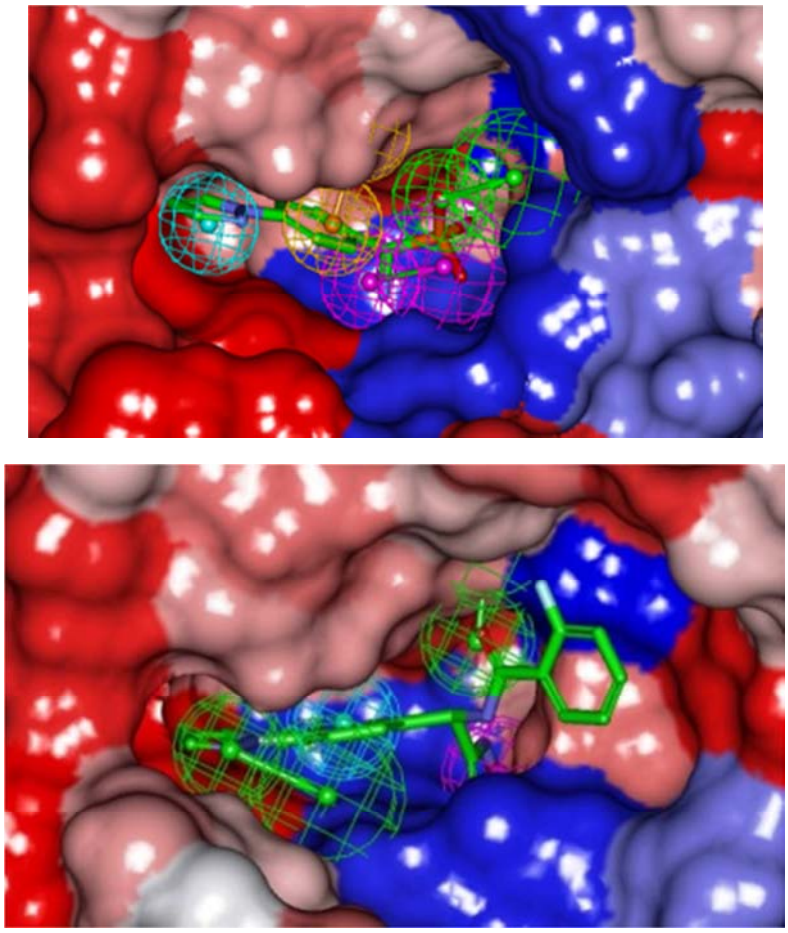

Figure 10. *pfA-M17 active-site Connolly surface with bound most active inhibitors APP1 (left) and AHO1 (right) each one mapped to its PH4. The binding site surface is colored according to residue hydrophobicity: red – hydrophobic, blue – hydrophilic, and white – intermediate.*

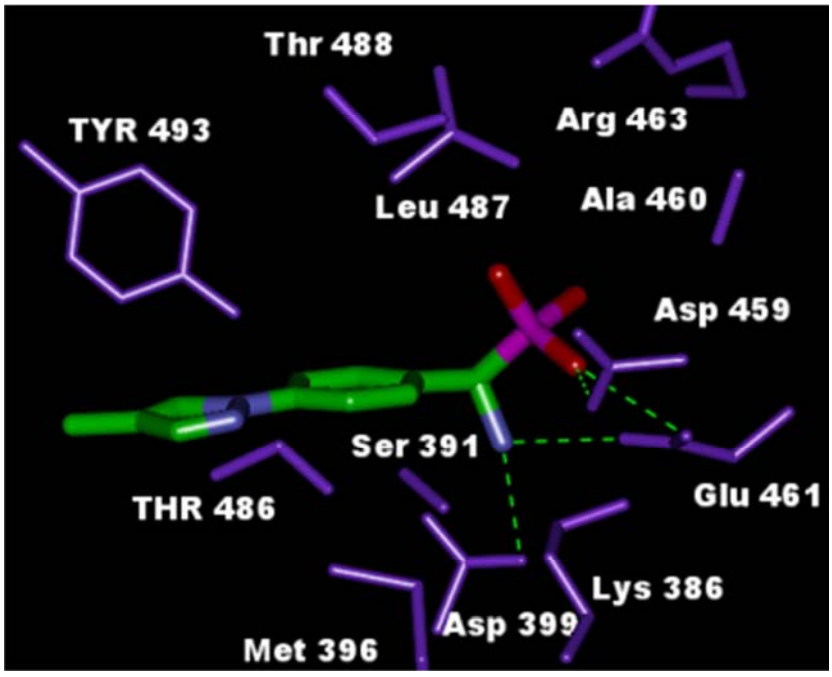

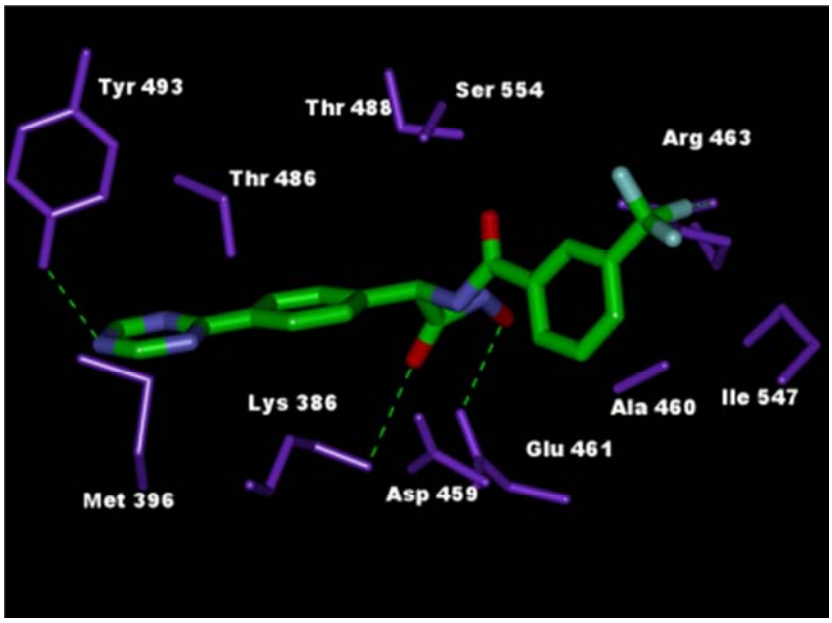

Figure 11. *Enzyme – ligand interactions at the active site of pfA-M17 depicted in 3D for the best APP analogue (left), AHO (right).*

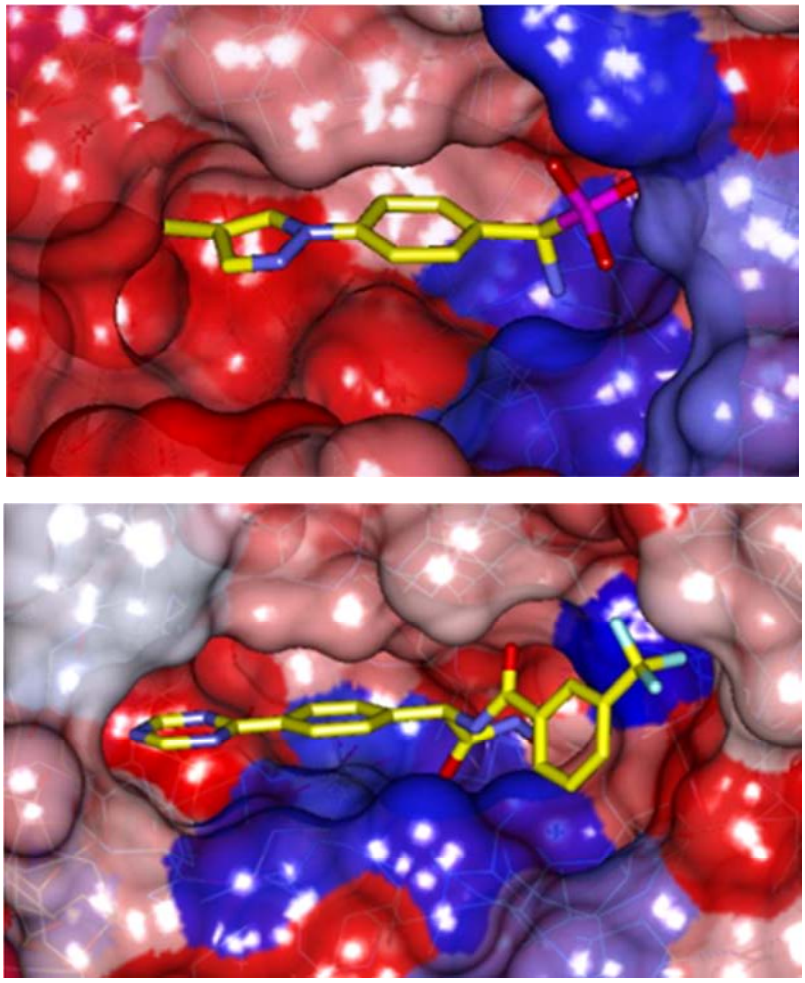

Figure 12. *Connolly surface of the active-site of pfA-M17 with bound best APP analogue (left), AHO (right). The binding site surface is colored according to residue hydrophobicity: red – hydrophobic, blue – hydrophilic, and white – intermediate.*

Table 13. *R-groups (fragments, building blocks, substituents) used in the design of the initial diversity library of APP.*

R-groups				
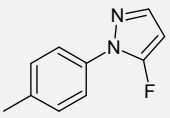	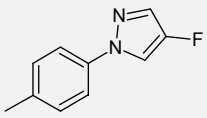	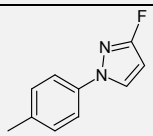	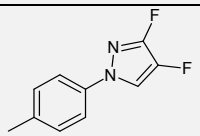	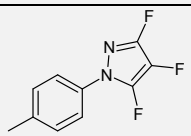
1	2	3	4	5
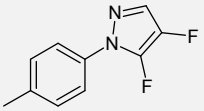	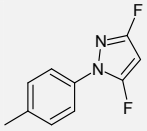	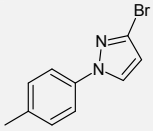	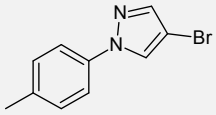	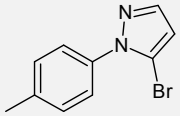
6	7	8	9	10
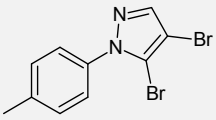	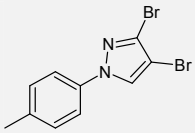	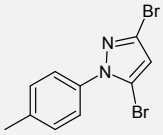	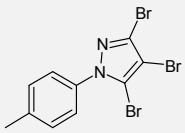	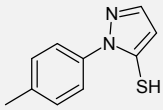
11	12	13	14	15
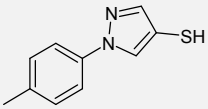	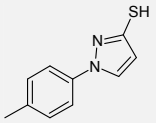	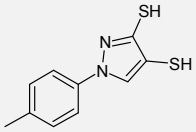	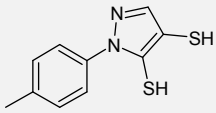	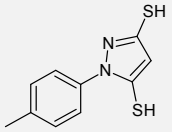
16	17	18	19	20
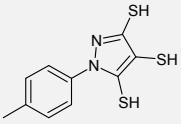	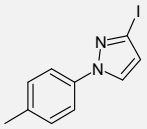	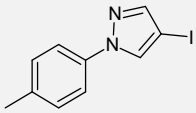	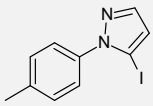	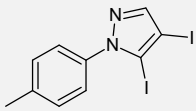
21	22	23	24	25
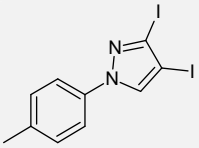	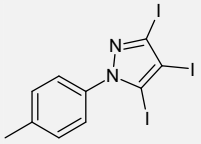	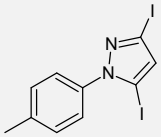	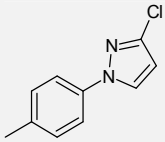	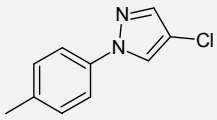
26	27	28	29	30
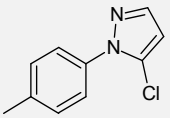	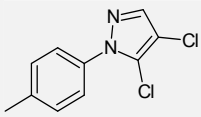	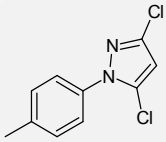	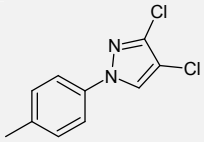	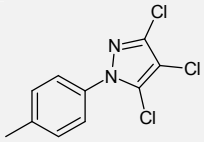
31	32	33	34	35
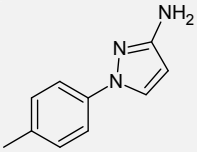	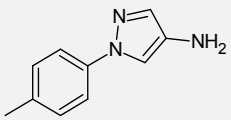	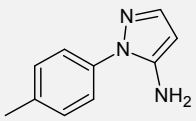	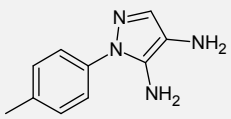	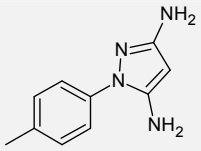
36	37	38	39	40
41	42	43	44	45
46	47	48	49	50

R-groups

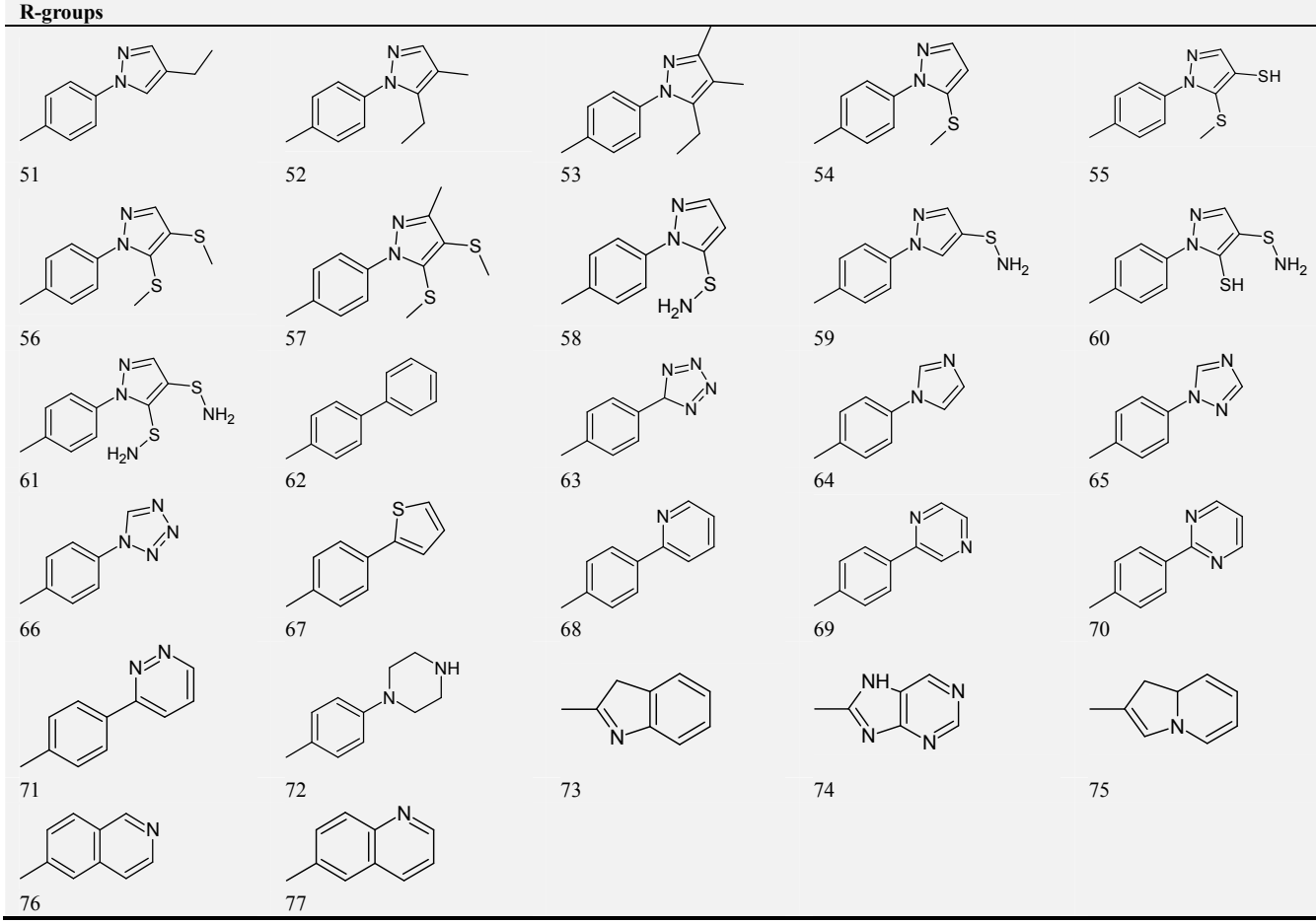

Table 14. *APP analogues inhibitors of pfA-M17, the name is a concatenation APP-A-#R, #R is the R group numbering from table 13.*

Analogue (*)	M_w [b] [g mol^{-1}]	$\Delta\Delta H_{MM}$ [c] [kcal mol^{-1}]	$\Delta\Delta G_{sol}$ [d] [kcal mol^{-1}]	$\Delta\Delta TS_{vib}$ [e] [kcal mol^{-1}]	$\Delta\Delta G_{com}$ [f] [kcal mol^{-1}]	K_i [nM]
APP1		0	0	0	0	11
APP-A-1	387	-4.33	2.29	-1.42	-0.61	3.4
APP-A-2	288	0.59	-0.49	-1.34	1.43	30.1
APP-A-6	322	-1.18	-2.61	-3	-0.7937	2.8
APP-A-20	317	-1.24	3.09	-0.59	2.44	873
APP-A-23	379	3.02	-1.33	-1.65	3.34	228
APP-A-30	271	-0.83	-2.15	-1.03	-1.95	0.8
APP-A-32	288	-5.72	2.73	-2.4	-0.59	3.5
APP-A-43	267	-0.06	-3.23	0.21	-3.49	0.15
APP-A-44	266	-0.58	0.60	1.97	-1.95	0.8
APP-A-50	281	1.23	-1.12	0.84	-0.7251	3
APP-A-58	300	1.53	-0.78	1.29	-0.5388	3.7
APP-A-59	331	5.85	-1.85	-0.41	4.41	711.6
APP-A-60	346	6.02	-3.98	-1.75	3.79	367.9
APP-A-61	263	-0.6	-1.95	0.94	-3.49	0.16
APP-A-73	228	4.36	-2.87	-5.15	6.64	7623.5
APP-A-76	237	2.83	0.68	-0.65	4.16	549.4

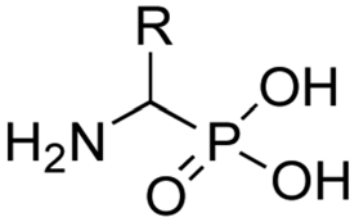

Table 15. *APP analogues inhibitors of pfA-M17, depicted in 2D, the name is a concatenation APP-A-#R, #R is the R group numbering from table 13.*

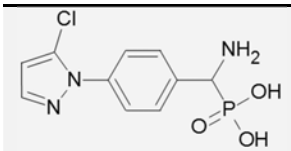 APP-A-1	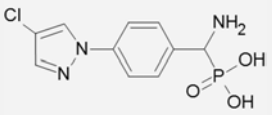 APP-A-2	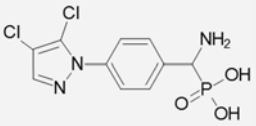 APP-A-6	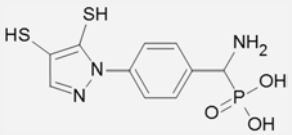 APP-A-20
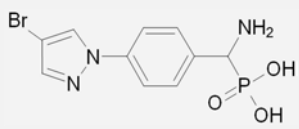 APP-A-23	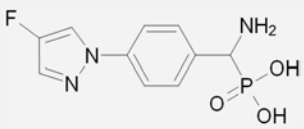 APP-A-30	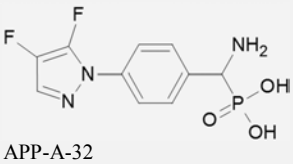 APP-A-32	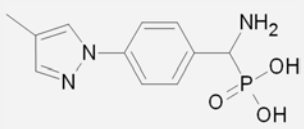 APP-A-43
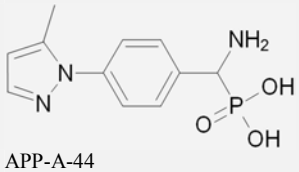 APP-A-44	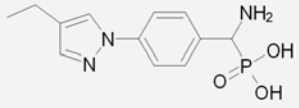 APP-A-50	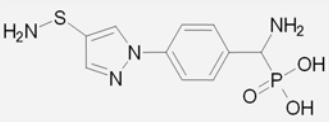 APP-A-58	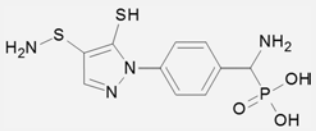 APP-A-59
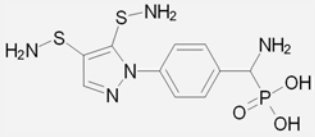 APP-A-60	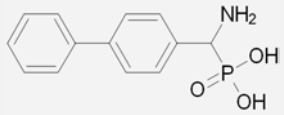 APP-A-61	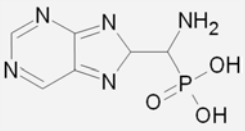 APP-A-73	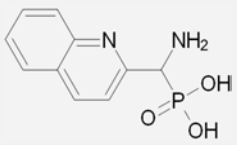 APP-A-76

Table 16. *R-groups (fragments, building blocks, substituents) used in the design of the initial diversity library of AHO analogues: R_1 (1 – 84) and R_2 (85 – 134).*

R-groups			
R_1			
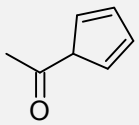 1	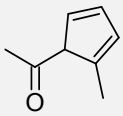 2	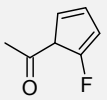 3	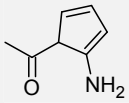 4
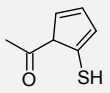 5	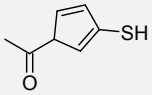 6	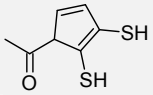 7	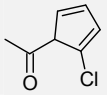 8
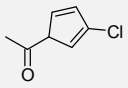 9	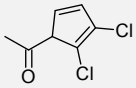 10	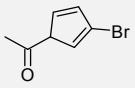 11	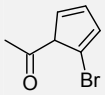 12
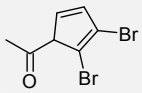 13	 14	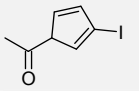 15	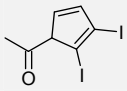 16
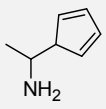 17	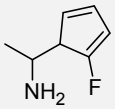 18	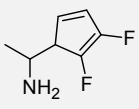 19	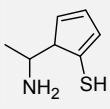 20
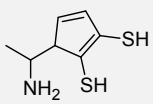 21	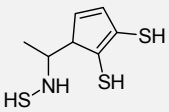 22	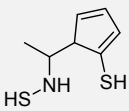 23	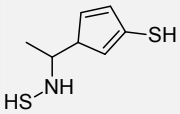 24
25	26	27	28

R-groups			
R_1			
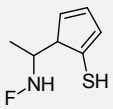	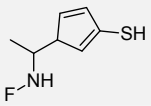	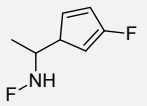	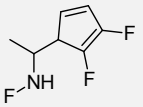
29	30	31	32
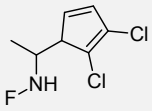	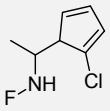	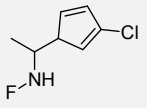	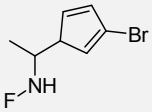
33	34	35	36
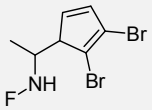	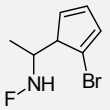	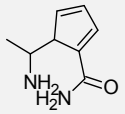	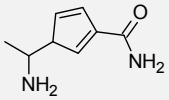
37	38	39	40
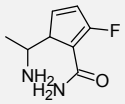	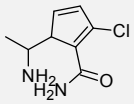	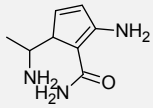	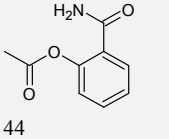
41	42	43	44
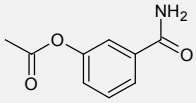	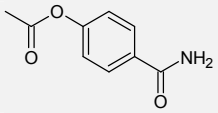	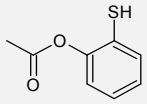	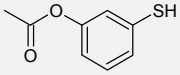
45	46	47	48
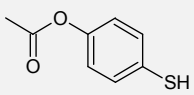	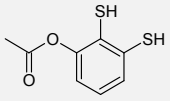	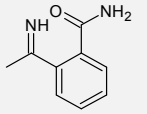	
49	50	51	52
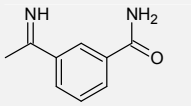	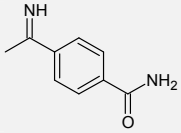	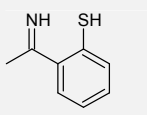	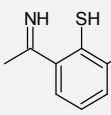
53	54	55	56
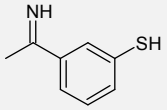	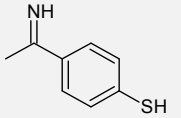	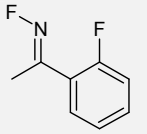	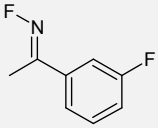
57	58	59	60
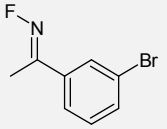	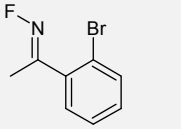	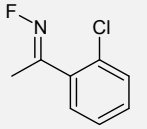	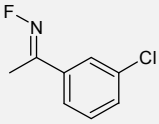
61	62	63	64
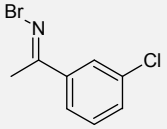	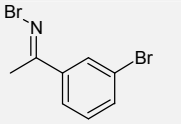	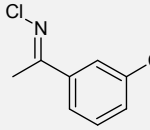	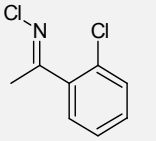
65	66	67	68
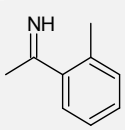			
69	70	71	72

R-groups			
R_1			
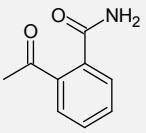	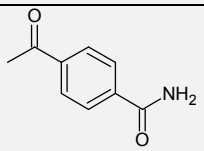	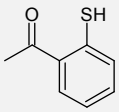	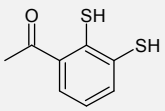
73	74	75	76
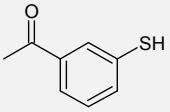	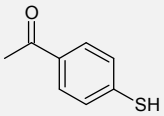	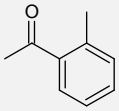	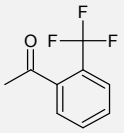
77	78	79	80
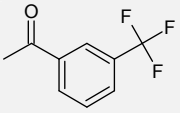	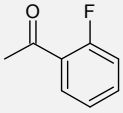	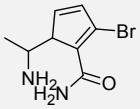	
81	82	83	84
R_2			
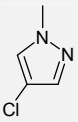	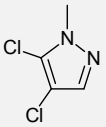	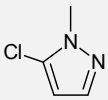	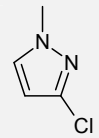
85	86	87	88
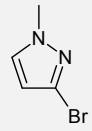	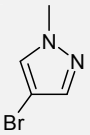	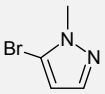	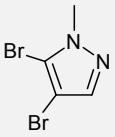
89	90	91	92
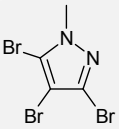	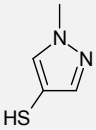	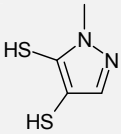	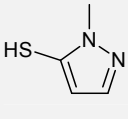
93	94	95	96
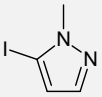	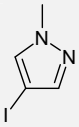	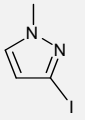	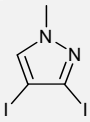
97	98	99	100
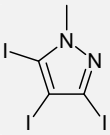	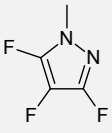	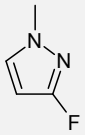	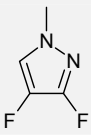
101	102	103	104
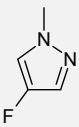	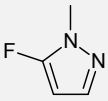	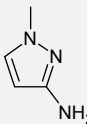	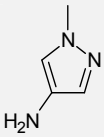
105	106	107	108
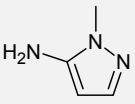	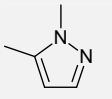	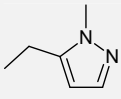	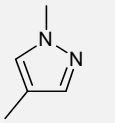
109	110	111	112
113	114	115	116

R-groups			
R_1			
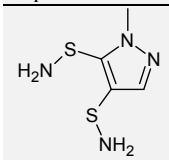	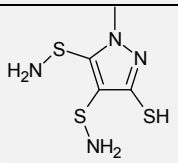	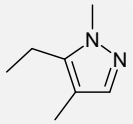	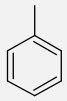
117	118	119	120
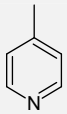	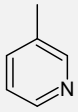	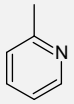	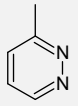
121	122	123	124
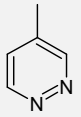	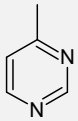	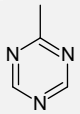	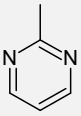
125	126	127	128
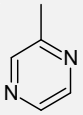	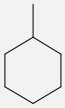	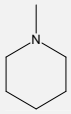	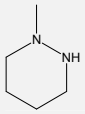
129	130	131	132
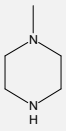	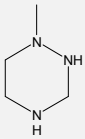		
133	134		

Table 17. *AHO analogues with scaffold A, the name is a concatenation A-#R_1-#R_2, #R_1 and #R_2 being the R group numbering from table 16.*

Analogue (*)	M_w [b] [g mol^{-1}]	$\Delta\Delta H_{MM}$ [c] [kcal mol^{-1}]	$\Delta\Delta G_{sol}$ [d] [kcal mol^{-1}]	$\Delta\Delta TS_{vib}$ [e] [kcal mol^{-1}]	$\Delta\Delta G_{com}$ [f] [kcal mol^{-1}]	K_i [nM]
AHO1		0	0	0	0	8
A-4-117	434	-0.07	2.91	-0.3	3.14	36.7
A-6-118	482	2.9	-2.17	-0.94	1.67	20.9
A-7-127	401	-26.07	16.73	-1.6	-7.74	0.5
A-10-112	407	-7.41	2.96	-1.62	-2.83	3.7
A-10-133	411	4.31	3.91	3.1	5.12	78.3
A-12-108	465	-15.6	9.24	-1.53	-4.83	1.7
A-24-127	402	-9.86	20.67	2.35	8.46	281.9
A-26-125	387	-19.18	21.43	1.3	0.94	15.8
A-44-92	553	-10.5	0.94	-0.1	-9.46	0.29
A-44-93	773	-8.29	3.59	-3.17	-1.53	6.1
A-47-95	449	-0.71	1.94	-1.91	3.14	36.7
A-50-108	432	-7.62	1.24	2.04	-8.42	0.4
A-54-116	457	5.24	7.58	0.18	12.64	1401.8
A-74-127	392	-7.62	5.81	1.61	-3.42	2.9
A-77-92	526	-3.86	-2.65	-4.41	-2.1	4.9
A-81-127	417	-17.53	7.45	-0.54	-9.54	0.28
A-82-127	367	-10.94	6.07	-0.48	-4.39	2

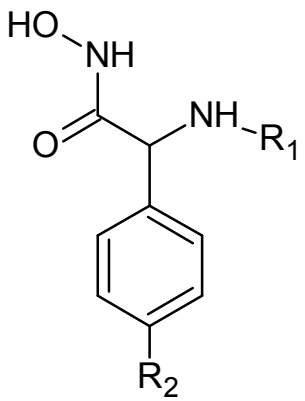

Table 18. *AHO analogues with scaffold A, depicted in 2D, the name is a concatenation A-#R_1-#R_2, #R is the R group numbering from table 16.*

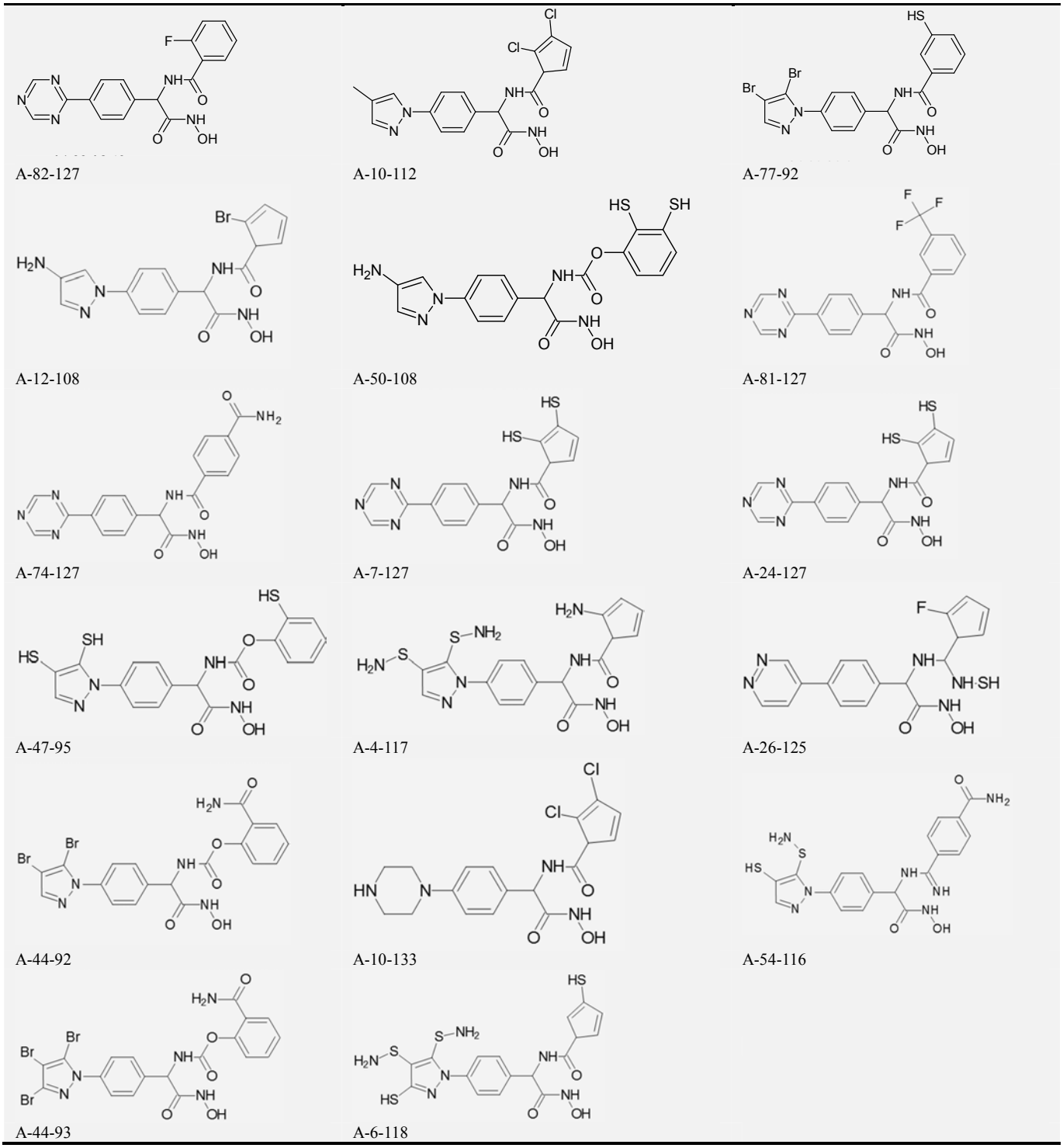

Table 19. *Predicted ADME-related properties of the best-designed APP analogues.*

APP[a]	#stars[b]	M_W [g/mol]	Smol[d] [Å^2]	Smol, hfo[e] [Å^2]	Vmol[f] [Å^3]	RotB[g]	HB don[h]	HB acc[i]	logPo/w [j]
APP-A-1	0	287.6	462.2	15.1	780.4	5	4	7	-1.1
APP-A-44	0	267.2	473	94.1	798.0	5	4	7	-1.2
APP-A-32	0	289.1	471.1	15.2	783.1	5	4	7	-1.0
APP-A-61	0	263.2	498.4	12.7	834.1	6	4	6	-0.6
APP-A-43	0	267.2	498.4	106.3	835.0	5	4	7	-1.2
APP-A-30	0	271.1	474.5	12.5	790.0	5	4	7	-1.2
APP-A-50	0	281.2	531.5	149.2	891.1	6	4	7	-0.9
APP-A-6	0	322.1	507.7	12.6	853.3	5	4	7	-0.6

Table 19. *Continued.*

APP[a]	logSwat[k]	logKHSA[l]	logB/B[m]	BIPcaco[n] [nm.s^{-1}]	#*meta* [o]	Ki [pred]	HOA[q]	%HOA[r]
APP-A-1	-1.6	-0.94	-0.8	2.4	3	3.4	1	27.3
APP-A-44	-1.5	-0.92	-1.0	2.4	4	0.8	1	26.6
APP-A-32	-1.8	-0.96	-0.8	2.4	3	3.5	1	27.8
APP-A-61	-1.8	-1.04	-0.8	2.90	3	0.16	1	31.9
APP-A-43	-1.8	-1.17	-0.9	1.80	4	0.15	1	25.0
APP-A-30	-1.7	-0.99	-1.0	1.90	3	0.8	1	25.0
APP-A-50	-2.1	-1.30	-0.8	1.90	4	3	1	26.9
APP-A-6	-2.5	-0.87	-0.9	1.90	3	2.8	1	28.3

[a]best designed APPs analogues, Table 15;
[b]drug likeness, number of property descriptors (from 24 out of the full list of 49 descriptors of QikProp, ver. 3.7, release [14]) that fall outside of the range of values for 95% of known drugs;
[c]molecular weight in g.mol^{-1} (range for 95% of drugs: 130 - 725 g.mol^{-1}) [14];
[d]total solvent-accessible molecular surface, in Å^2 (probe radius 1.4 Å) (range for 95% of drugs: 300 - 1000 Å^2);
[e]hydrophobic portion of the solvent-accessible molecular surface, in Å^2 (probe radius 1.4 Å) (range for 95% of drugs: 0 - 750 Å^2);
[f]total volume of molecule enclosed by solvent-accessible molecular surface, in Å^3 (probe radius 1.4 Å) (range for 95% of drugs: 500 - 2000 Å^3);
[g]number of non-trivial (not CX3), non-hindered (not alkene, amide, small ring) rotatable bonds (range for 95% of drugs: 0 - 15);
[h]estimated number of hydrogen bonds that would be donated by the solute to water molecules in an aqueous solution. Values are averages taken over a number of configurations, so they can be non-integer (range for 95% of drugs: 0.0 - 6.0);
[i]estimated number of hydrogen bonds that would be accepted by the solute from water molecules in an aqueous solution. Values are averages taken over a number of configurations, so they can be non-integer (range for 95% of drugs: 2.0 - 20.0);
[j]logarithm of partitioning coefficient between n-octanol and water phases (range for 95% of drugs: -2 - 6.5);
[k]logarithm of predicted aqueous solubility, log S. S in mol dm^{-3} is the concentration of the solute in a saturated solution that is in equilibrium with the crystalline solid (range for 95% of drugs: -6.0 - 0.5);
[l]logarithm of predicted binding constant to human serum albumin (range for 95% of drugs: -1.5 - 1.5);
[m]logarithm of predicted brain/blood partition coefficient. Note: QikProp predictions are for orally delivered drugs so, for example, dopamine and serotonin are CNS negative because they are too polar to cross the blood-brain barrier (range for 95% of drugs: -3.0 - 1.2);
[n]predicted apparent Caco-2 cell membrane permeability in Boehringer-Ingelheim scale, in [nm/s] (range for 95% of drugs: < 25 poor, > 500 great);
[o]number of likely metabolic reactions (range for 95% of drugs: 1 - 8);
[p]predicted inhibition constants K_i^{pre}. K_i^{pre} was predicted from computed $\Delta\Delta G_{com}$ using the regression equation shown in Table 5;
[q]human oral absorption (1 - low, 2 - medium, 3 - high);
[r]percentage of human oral absorption in gastrointestinal tract (<25% - poor, >80% high);
[(*)]star indicating that the property descriptor value falls outside the range of values for 95% of known drugs.

Table 20. *Predicted ADME-related properties of the best-designed AHO analogues. For the legend see Table 19.*

AHO[a]	#stars[b]	M_W [g.mol^{-1}]	Smol[d] [Å^2]	Smol, hfo[e] [Å^2]	Vmol[f] [Å^3]	RotB[g]	HBdon[h]	HBacc[i]	logPo/w [j]
A-82-127	0	367.3	626.6	9.1	1080.3	6	2.2	9.4	0.62
A-10-112	0	407.2	647.7	148.9	1138.6	5	2.2	6.9	2.02
A-77-92	1	526.2	694.1	8.7	1207.7	6	3.1	7.4	2.7
A-50-108	0	431.4	723.1	7.6	1236.5	8	5.3	9.4	0.39
A-81-127	0	417.3	672.6	10.4	1167.1	6	2.2	9.4	1.3
A-7-127	0	401.4	627.1	55.4	1106.7	8	3.1	9.4	0.7
A-44-92	0	553.1	722.5	9.7	1271.1	6	4.2	9.9	0.97
Dapsone	1	236.2	431.6	0	687.9	2	0	7	-0.37
Trimethoprim	0	272.2	500.2	223.9	835.9	5	0	6.5	0.59
Chloroquine	1	293.7	594.1	188.9	982.9	6	0	3	4.56
Amodiaquine	1	333.7	603.2	131.7	1018.7	6	0	5	3.61
Mefloquine	2	362.2	533.1	0	925.1	2	0	4	4.14
pamaquine	0	315.5	654.8	443.4	1148.1	9	1	4.75	4.02
Sulfametopyrazine	1	268.2	473.4	77.8	773.3	4	0	9	-1.03
Tetracycline	5	422.3	604.5	173.1	1111.8	2	0	16	-3.43
Quinacrine	0	369.7	680.5	268.8	1163.6	7	0	3.5	5.57
Proguanil	1	237.6	478.2	125.3	768.6	6	0	6	1.09
Halofantrine	5	470.2	785.4	160.2	1351.8	5	0	3	7.63
Sulfadoxine	1	296.2	510.6	152.3	849.5	5	0	9.5	-0.79
Hydroxychloroquine	1	309.7	609.5	119.5	1006.5	6	0	5	3.36
Bulaquine	0	369.5	560.2	360.2	1097.8	9	1	5.8	3.62
Lumefantrine	5	496.7	819.1	160.7	1437.5	7	0	3	8.27
arteether	1	312.4	531.1	506.1	970.2	2	0	5.7	2.7
dihydroartemisinine	1	284.4	477.4	395.7	864.6	1	1	5.7	1.84
Doxycycline	4	422.3	602.2	174.1	1104.2	2	0	17.2	-3.99
Artemisinin	0	282	456.6	380.6	848.4	0	0	5.3	1.7

Table 20. *Continued.*

AHO[a]	logSwat[k]	logKHSA[l]	logB/B[m]	BIPcaco[n] [nm.s^{-1}]	#*meta* [o]	Ki[pred]	HOA[q]	%HOA[r]
A-82-127	-2.5	-0.78	-1.7	66.4	2	1.8	3	63
A-10-112	-4.1	-0.18	-1.4	78.1	3	3.3	3	73
A-77-92	-4.9	-0.19	-1.1	115.1	2	4.3	3	67.1
A-50-108	-2.9	-0.65	-2.1	4.3	3	0.4	2	40.6
A-81-127	-3.6	-0.6	-1.6	63.7	3	0.2	3	67.3
A-7-127	-2.5	-0.78	-1.8	41.2	5	0.4	2	59.9
A-44-92	-4.2	-0.48	-2.5	9.9	2	0.3	2	37.5
Dapsone	-0.5	-1.34	-0.9	289.1	0		2	68.8
Trimethoprim	-1.5	-0.91	-1.2	282.8	3		3	74.3
Chloroquine	-5.3	0.41	-0.1	3718.1	0		3	100
Amodiaquine	-4.4	-0.02	-0.4	1689.1	0		3	100
Mefloquine	-4.9	0.15	0.5	2903.1	0		3	100
pamaquine	-3.8	0.43	0.2	1475.2	5		3	100
Sulfametopyrazine	0.2	-1.7	-1.3	195.8	1		2	61.9
Tetracycline	1.1	-2.5	-2.6	6.8	5		1	21.8
Quinacrine	-6.5	0.8	-0.1	4435.7	1		1	100
Proguanil	-1.5	-1.1	-0.7	834.6	0		3	85.6
Halofantrine	-9.9	1.5	0.2	2844.1	0		1	100
Sulfadoxine	-0.11	-1.7	-1.4	213.4	2		2	63.9
Hydroxychloroquine	-4.51	-0.1	-0.7	1023.7	0		3	100
Bulaquine	-2.98	0.1	-0.4	3099.7	7		3	100
Lumefantrine	-10.01	1.7	0.2	4337.2	0		1	100
arteether	-2.99	-0.2	0.2	5731.8	0		3	100
dihydroartemisinine	-2.92	-0.1	-0.1	1664.9	0		3	95.4
Doxycycline	1.73	-2.88	-2.45	9.17	4		1	20.8
Artemisinin	-2.1	-0.3	0.001	1886	1		3	95.8

References

[1] The Millennium Development Goals Report, 2015, http://www.un.org/millenniumgoals.

[2] M. Kyaw, I. Mallika, M. Khin, A. Aye, M. Tin, L. Thaung H, L. Khin, P. Myat, P. Katherine, M. Abul, D. Mehul, Y. Phaik, P. Sasithon, A. Elizabeth, J. Tim, N. Shalini, M. Marina, A. Jennifer, P. Eric, G. Philippe, J. Richard, S. Frank, M. Arjen, P. Nicholas, N. François, J. Nicholas and J. Charles. Spread of artemisinin-resistant *Plasmodium falciparum* in Myanmar: a cross-sectional survey of the K13 molecular marker. 2015, 15, 415–421.

[3] A. Mbengue, S. Bhattacharjee, T. Pandharkar, H. Liu, G. Estiu, R. Stahelin, S. Rizk, D. Njimoh, Y. Ryan, K. Chotivanich, C. Nguon, M. Ghorbal, J. Rubio, M. Pfrender, S. Emrich, N. Mohandas, A. Dondorp, O. Wiest and K. Haldar, A molecular mechanism of artemisinin resistance in *Plasmodium falciparum* malaria, *Nature*, vol. 520, 2015, pp. 683–687.

[4] R. Capela et al., "Artemisinin-dipeptidyl vinyl sulfone hybrid molecules: Design, synthesis and preliminary SAR for antiplasmodial activity and falcipain-2 inhibition," *Bioorganic and Medicinal Chemistry,* vol. 19, 2009, pp. 3229-3232.

[5] M. Muregi F and A. Ishih, "Next-generation antimalarial drugs: hybrid molecules as a new strategy in drug design," *Drug Development Research,* vol. 71, 2010, pp. 20−32.

[6] S. Chauhan, M. Sharma, and P. Chauhan, "Trioxaquines: hybrid molecules for the treatment of malaria," *Drug News Perspect,* vol. 23, 2010, pp. 632−646.

[7] E. Cunningham, M. Drag, P. Kafarski and A. Bell, "Chemical target validation studies of aminopeptidase in malaria parasites using α-aminoalkyl phosphonate and phosphonopeptide inhibitors,"*Antimicrob Agents Chemother,* vol. 52, 2008, pp. 3221–3228.

[8] S. Skinner-Adams, J. Lowther, F. Teuscher, M. Stack, J. Grembecka, A. Mucha, P. Kafarski, K. Trenholme, P. Dalton and D. Gardiner, "Identification of phosphinate dipeptide analogue inhibitors directed against the Plasmodium falciparum M17 leucine aminopeptidase as lead antimalarial compounds, "*Journal of Medicinal Chemistry, vol.* 50, 2007, pp. 6024–6031.

[9] S. McGowan, A. Oellig, A. Birru, T. Caradoc-Davies, M. Stack, J. Lowther, T. Skinner-Adams, A. Mucha, P. Kafarski, J. Grembecka, R. Trenholme, M. Buckle, L. Gardiner, P. Dalton and C. Whisstock, "Structure of the Plasmodium falciparum M17 aminopeptidase and significance for the design of drugs targeting the neutral exopeptidases," *PNAS*, vol. 107, 2010, pp. 2449–2454.

[10] M. Klemba, I. Gluzman and DE. Goldberg, "A Plasmodium falciparum dipeptidyl aminopeptidase I participates in vacuolar hemoglobin degradation", *Journal of Biological Chemistry*, vol. 279, 2004, pp. 43000−43007.

[11] M. Stack, J. Lowther, E. Cunningham, S. Donnelly, L. Gardiner, R. Trenholme, S. Skinner-Adams, F. Teuscher, J. Grembecka, A. Mucha, P. Kafarski, L. Lua, A. Bell and P. Dalton, "Characterization of the Plasmodium falciparum M17 leucyl aminopeptidase. A protease involved in amino acid regulation with potential for antimalarial drug development," *Journal of Biological Chemistry,* vol. 282, 2007, pp. 2069−2080.

[12] K. Sivaraman, A. Paiardini, M. Sieńczyk, C. Ruggeri, A. Oellig, P. Dalton, J. Scammells, M. Drag and S. McGowan, "Synthesis and Structure−Activity Relationships of Phosphonic Arginine Mimetics as Inhibitors of the M1 and M17 Aminopeptidases from Plasmodium falciparum," *Journal of Medicinal Chemistry,* vol. 56, 2013, pp. 5213−2017.

[13] N. Shailesh, N. Drinkwater, C. Ruggeri, K. Sivaraman, S. Loganathan, S. Fletcher, M. Drag, A. Paiardini, M. Avery, J. Scammells and S. McGowan, "Two-Pronged Attack: Dual Inhibition of Plasmodium falciparum M1 and M17 Metalloaminopeptidases by a Novel Series of Hydroxamic Acid-Based Inhibitors," *Journal of Medicinal Chemistry,* vol. 57, 2014, pp. 9168−9183.

[14] QikProp, version 3.7, release 14, X Schrödinger, LLC, New York, NY, 2014.

[15] V. Frecer, M. Kabelac, P. De Nardi, S. Pricl and S. Miertus, "Structure-based design of inhibitors of NS3 serine protease of hepatitis C virus," *Journal of Molecular Graphics and Modelling*, vol. 22, 2004, pp. 209–220.

[16] V. Frecer, A. Jedinak, A Tossi, F. Berti, F. Benedetti, D. Romeo and S. Miertus, "Structure based design of inhibitors of aspartic protease of HIV-1," *Letters in Drug Design Discovery,* vol. 2, 2005, pp. 638–646.

[17] V. Frecer, F. Berti, F. Benedetti, S. Miertus, "Design of peptidomimetic inhibitors of aspartic protease of HIV-1 containing -PheΨPro- core and displaying favourable ADME-related properties," *Journal of Molecular Graphics Modelling,* vol. 27, 2008, pp. 376–387.

[18] B. Dali, M. Keita, E. Megnassan, V. Frecer, S. Miertus,"Insight into selectivity of peptidomimetic inhibitors with modified statine core for plasmepsin II of *Plasmodium falciparum* over human cathepsin D," *Chemical Biology and Drug Design,* vol. 79, 2012, pp. 411-430.

[19] E. Megnassan, M. Keita, C. Bieri, A. Esmel, V. Frecer et al., "Design of novel dihydroxynaphthoic acid inhibitors of *Plasmodium falciparum* lactate dehydrogenase," *Medicinal Chemistry*, vol. 8, 2012, pp. 970-984.

[20] C. Owono Owono, M. Keita, E. Megnassan, V. Frecer, S. Miertus, "Design of thymidine analogues targeting thymidilate kinase of *Mycobacterium tuberculosis*," *Tuberculosis Research and Treatment*, 2013, 670836.

[21] M. Keita, A. Kumar, B. Dali, E. Megnassan, M. I. Siddiqi, V. Frecer, S. Miertus, "Quantitative structure- activity relationships and design of thymine-like inhibitors of thymidine monophosphate kinase of *Mycobacterium tuberculosis* with favourable pharmacokinetic profiles," *Royal Society Chemistry*, vol. 4, 2014, pp. 55853-55866.

[22] V. Frecer, P. Seneci, S. Miertus, "Computer-assisted combinatorial design of bicyclic thymidine analogues as inhibitors of Mycobacterium tuberculosis thymidine monophosphate kinase," *Journal of Computer-Aided Molecular Design*. Vol. 25, 2011, pp. 31–49.

[23] L. C. Owono Owono, F. Ntie-Kang, M. Keita, E. Megnassan, V. Frecer and S. Miertus, "Virtually Designed Triclosan - Based Inhibitors of Enoyl - Acyl Carrier Protein Reductase of *Mycobacterium tuberculosis* and of *Plasmodium falciparum*," *Molecular Informatics*, vol. 34, 2015, pp. 292–307.

[24] F. Kouassi, M. Kone, M. Keita, A. Esmel, E. Megnassan, V. Frecer, T. Y. N'Guessan and S Miertus. "Computer-Aided Design of Orally Bioavailable Pyrrolidine Carboxamide Inhibitors of Enoyl-Acyl Carrier Protein Reductase of Mycobacterium tuberculosis with Favorable Pharmacokinetic Profiles," *International Journal of Molecular Sciences*, vol. 16, 2015, pp. 29744–29771.

[25] H. M. Berman, J. Westbrook, Z. Feng, G. Gilliland, T. N. Bhat et al. "The protein data bank," *Nucleic Acids Research*, vol. 28, 2000, pp. 235–242.

[26] Insight-II and Discover molecular modeling and simulation package, version 2005, Accelrys, San Diego, Calif, USA, 2005.

[27] Discovery Studio molecular modeling and simulation program, version 2.5, Accelrys, San Diego, Calif, USA, 2009.

[28] Molecular Operating Environment (MOE), 2014. 10. Chemical Computing Group Inc, 1010 Sherbooke St West, Suite #910, Montreal, QC, Canada, H3A 2R7, 2009.

[29] Available Chemicals Directory, Version 95.1, MDL Information Systems, San Leandro, CA.

[30] C. A. Lipinski, F. Lombardo, B. W. Dominy, P. J. Feeney, "Experimental and computational approaches to estimate solubility and permeability in drug discovery and development settings," *Advanced Drug Delivery Reviews*, vol. 46, 2001, pp. 3–26.

[31] T. S. Skinner-Adams, J. Lowther, F. Teuscher, C. M. Stack, J. Grembecka, A. Mucha, et al. Identification of phosphinate dipeptide analog inhibitors directed against the *Plasmodium falciparum* M17 leucine aminopeptidase as lead antimalarial compounds. *J Med Chem* vol. 50, 2007, pp. 6024–31.